Environ Earth Sci
DOI 10.1007/s12665-013-2630-6

ORIGINAL ARTICLE

Characterisation of the Sarcheshmeh copper mine tailings, Kerman province, southeast of Iran

Sajjad Jannesar Malakooti · Seyed Ziaedin Shafaei Tonkaboni · Mohammad Noaparast · Faramarz Doulati Ardejani · Reza Naseh

Received: 8 January 2013 / Accepted: 24 June 2013

Abstract Mineral processing operation at the Sarcheshmeh porphyry copper mine has produced huge quantities of tailings materials containing sulphide minerals in particular pyrite. These tailings materials were geochemically and mineralogically characterised to assess pyrite and chalcopyrite oxidation, acid mine drainage generation, and trace element mobility to lead development of a proper remediation plan. Five vertical trenches up to 4.2 m deep were excavated from the tailings surface, and 70 solid samples were taken in 0.3 m intervals. The samples were first mineralogically analysed. Pyrite was the main sulphide mineral found in the tailings. The gangue minerals include quartz ± muscovite–illite ± chlorite ± albite ± orthoclase ± halite. The samples were geochemically analysed for total concentrations of 62 elements, paste pH, SO_4^{2-}, CO_3^{2-}, and HCO_3^-. The maximum concentrations of SO_4^{2-} (1,300, 1,170, 1,852, 1,960 and 837 mg/L) were observed at a depth of 0.9 m in profiles A, B, C, D and E, respectively. The tailings have a high acid-producing potential and low acid-neutralising potential (pyrite 4–6 wt %, calcite 1 wt %). $Fe_2(SO_4)_3$, $CuSO_4$, $MgSO_4$ and $MnSO_4$ were the dominant secondary sulphate minerals in the tailings. The lowest pH values (2.9, 3 and 3) were measured at a depth of 0.3 m in the profiles A, B and C, 3.9 at a depth of 0.6 m in the profile D and 3 at a depth of 0.9 m in the profile E. The upper portions of the profiles C (1.8 m) and D (2.1 m) were moderately oxidised, while oxidation in the profiles A, B and E did not extend more than 1.2, 1.2 and 1.5 m beneath the tailings surface. Zn, Pb, Rb, U, Hf, Nd, Zr and Ga show almost a constant trend with depth. Cd, Sr, Th, La and Ce increased with increasing depth of the tailings materials while, Co, V, Ti, Cr, Cu, As, Mn, Ag, Mo and Ni exhibit initially a decreasing trend from tailings surface to the depths that vary between 0.9 and 1.2. They then remained constant with the depth. The results show pyrite and chalcopyrite oxidation at surface layers of the tailings and subsequent leaching of the oxidation products and trace elements by infiltrated atmospheric precipitation.

Keywords Tailings · Sarcheshmeh copper mine · Mineral processing plant · Pyrite and chalcopyrite oxidation · Geochemical characterisation · Trace elements

Introduction

The Sarcheshmeh copper mine is located in the Central Iranian Volcanic Belt (CIVB), in Kerman Province, southeast of Iran (Shahabpour and Doorandish 2008). Mining activity and mineral processing operation have produced huge amounts of low-grade wastes and tailings materials that can cause many environmental problems (Doulati Ardejani et al. 2008a). The tailings materials in the Sarcheshmeh mine contain reactive sulphide minerals in particular pyrite (Jannesar Malakooti et al. 2012). When pyrite and other sulphide minerals are exposed to atmosphere and/or water, they undergo rapid oxidation that produce acid mine

S. Jannesar Malakooti (✉)
Department of Mining Engineering, Science and Research Branch, Islamic Azad University, Tehran, Iran
e-mail: s.jannesar@srbiau.ac.ir

S. Z. Shafaei Tonkaboni · M. Noaparast · F. Doulati Ardejani
School of Mining, College of Engineering, University of Tehran, Tehran, Iran

R. Naseh
National Iranian Copper Industries Company (NICICo.), Tehran, Iran

Published online: 16 July 2013

drainage (AMD) (Ricca and Schultz 1979; Atkins and Pooley 1982; Adam et al. 1997; Canovas et al. 2007; Zhao et al. 2007). The enhancement of sulphide minerals' oxidation principally pyrite (FeS_2) by mining activities is a worldwide problem. The Sarcheshmeh copper mine, in Kerman province, southeast Iran, provides a great opportunity to investigate the processes involved in sulphide mineral oxidation and AMD generation within sulphide-bearing tailings.

Pyrite is the most common sulphide mineral at the Earth's surface and is an important agent of electron cycling in the near surface environment. Weathering of pyrite is estimated at 36×10^{12} g/year, involving 0.02 mol of electrons per square metre of land-surface area. This current often drives other processes such as AMD generation, mobilisation and redox cycling of metals in sediments from mining and other environments, degradation of pollutants, reduction of aqueous trace metal complexes to form ore deposits. Pyrite oxidation is also important in technological applications ranging from hydrometallurgy to solar energy conversion (Carrick et al. 1996).

Two main oxidants (O_2 and Fe^{3+}) have been identified in AMD environments and necessary rate laws have been developed by many researchers (Singer and Stumm 1970; Williamson and Rimstidt 1994). Reaction mechanisms are less well known. Predicting and controlling the environmental aspects of pyrite oxidation (Carrick et al. 1996) require a better understanding of the chemical reactions involved.

The stoichiometric reaction describing pyrite oxidation and AMD generation is given by Eq. (1) (Stumm and Morgan 1996):

$$2FeS_2 + 7O_2 + 2H_2O \Rightarrow 2Fe^{2+} + 4SO_4^{2-} + 4H^+ \quad (1)$$

As Eq. 1 shows, pyrite is initially oxidised by the atmospheric O_2, producing H^+, SO_4^{2-}, and Fe^{2+} (Singer and Stumm 1970; Doulati Ardejani et al. 2008b).

Fe(II) may be further oxidised by O_2 into Fe(III) according to Eq. (2):

$$Fe^{2+} + \frac{1}{4}O_2 + H^+ \rightarrow Fe^{3+} + \frac{1}{2}H_2O \quad (2)$$

The ferric iron (Fe^{3+}) in turn either oxidises pyrite at low pH (Eq. 3) to produce additional Fe^{2+}, SO_4^{2-} *and* H^+or hydrolyses into amorphous iron hydroxide, accompanied by the release of additional H^+ ions into the environment at pH values greater that 3.5 (Eq. 4).

$$FeS_2 + 14Fe^{3+} + 8H_2O \Rightarrow 15Fe^{2+} + 2SO_4^{2-} + 16H^+ \quad (3)$$

$$Fe^{3+} + 3H_2O \rightarrow Fe(OH)_3 + 3H^+ \quad (4)$$

The oxygen-rich water used for copper processing in conjunction with rainwater and atmospheric exposure of tailings provide a best scenario for pyrite oxidation to occur in tailings materials. The pyrite oxidation rate highly depends on the temperature, pH, acidophilic Fe microorganisms, moisture and the availability of oxygen within the tailings, which is mainly governed by gaseous diffusion process (Schippers et al. 2007).

AMD with high concentrations of iron, SO_4 and low pH can carry potentially toxic metals such as As, Cd, Cu, Co, Mo, Ni, Pb and Zn and other dissolved materials away from the tailings site (Williams 1975). AMD has detrimental effects on soils, surface and groundwater (Williams 1975; Erickson et al. 1982; Walter et al. 1994a, b; Rubio and Olmo 1995; Dinelli et al. 2001; Banks and Banks 2001; Kim and Chon 2001; Moncur et al. 2005; Lee and Chon 2006; Canovas et al. 2007; Wu et al. 2009; Equeenuddin et al. 2010; Shafaei Tonkaboni et al. 2011; Jannesar Malakooti et al. 2012).

Many physical, chemical and biological processes are involved in sulphide minerals' oxidation and subsequent AMD generation. They include transport of atmospheric oxygen through the waste materials, chemical oxidation of sulphide minerals, bacterially mediated oxidation reaction, pH-buffering reactions due to dissolution of mineral phases, precipitation of secondary minerals, transportation of the oxidation products through the tailings and their interaction with solid phase (Morin et al. 1988; Shafaei Tonkaboni et al. 2011). Investigation into such processes provides useful information in developing an appropriate treatment plan and environmental management programme for tailings sites.

Kovács et al. (2012) performed a geochemical and mineralogical study of surface water and sediment at an abandoned lead and zinc mining area at Gyongyosoroszi in Hungary to investigate the role of potentially toxic elements in the contamination of the Toka stream. The drainage of the mine is characterised as neutralised acidic mine drainage. The amorphous iron hydroxide was the main secondary mineral found in the sediment. They observed the elevated concentrations of Zn, Cd, As and Pb. Moreover, the concentrations of As, Cd, Cu, Hg, Pb and Zn were high at the abandoned mine tailings as the secondary contamination source. These researches concluded that the quality of the Toka stream was not significantly influenced by the mining site. However, the high concentrations of Zn and Cd can be a potential risk for stream pollution.

Shahhoseiny et al. (2013) performed geochemical and mineralogical investigations in a pyritic waste pile at the Anjir Tangeh coal washing plant in northern Iran. Their study revealed that pyrite is oxidised at the upper portion of the pile. The oxidation process decreased sharply at depths of up to 1 m where the oxygen concentration decreased rapidly. They further showed that the wastes have low acid-producing potential and high acid-neutralising potential.

Pyrite and other sulphide minerals' oxidation and ensuing AMD generation are important processes that may take place within the wastes and tailings produced by copper mining and processing operations at the Sarcheshmeh mine. The mine site is characterised by appropriate climatic conditions that favour pyrite and chalcopyrite oxidation. A basic study of the geochemistry of tailings and a detailed investigation of AMD generation within the tailings can help to predict the likely long-term environmental impacts of the copper processing operation.

Many research works have been previously conducted in the Sarcheshmeh copper mine to investigate pollution problems, remove trace elements from AMD and predict heavy metals from AMD applying intelligent techniques (Marandi et al. 2010; Seifpanahi Shabani et al. 2011; Rooki et al. 2011; Soleimanifar et al. 2011; Gholami et al. 2011a, b; Ariafar et al. 2012). Literature review indicates that few works have been done to characterise the Sarcheshmeh copper mine tailings (Jannesar Malakooti et al. 2012). There is therefore a need to investigate sulphide minerals' oxidation in a large tailings impoundment at the Sarcheshmeh mine in Iran in detail. The main objectives of the research were to: geochemically and mineralogically characterise tailings materials at the Sarcheshmeh copper mine, investigate primary and secondary minerals, determine the level of pyrite and chalcopyrite oxidation, determine the mobility of trace elements, and eventually provide new data for further environmental programmes.

Site description

The tailings site in the Sarcheshmeh copper mine is located about 160 km southwest of Kerman and about 50 km southwest of Rafsanjan in the province of Kerman, in northeast of Iran (Fig. 1). The tailings site has an average elevation of 2,200 m. The main access road to the study area is Kerman–Rafsanjan–Shahr-E-Babak road. The average annual precipitation at the site varies between 300 and 550 mm. The temperature varies from +35 °C in summer to −20 °C in winter. The area is covered with snow about 3–4 months per year. The wind speed sometimes exceeds 100 km/h (Doulati Ardejani et al. 2008a).

In geological point of view, the ore body in the Sarcheshmeh is elliptical in shape with a length of about 2,300 m and a width of about 1,200 m. This ore body is centred on the late Tertiary Sarcheshmeh grano-diorite porphyry stock (Waterman and Hamilton 1975). The porphyry is a member of a complex series of magmatically related intrusive emplaced in the Tertiary volcanic rocks in a short distance from the edge of an older near batholith-sized grano-diorite mass. This deposit is recognised to be the fourth largest porphyry copper mine in the world consisting of 1 billion tonnes copper (0.9 %) and molybdenum (0.03 %) (Banisi and Finch 2001). The mineral processing operation in the Sarcheshmeh mine has produced and dumped more than 24 Mt of tailings in the study area. The tailings, which are approximately 12 m in height, cover an area of about 4 km^2 in 2012 (Fig. 2).

Materials and methods

Sampling and sample preparation

Altogether, 70 solid samples, 2 kg each in weight were taken in 0.3 m intervals from 5 trenches excavated in the tailings site (Trenches A, B, C, D and E in Fig. 1). The samples were placed in separate plastic bottles to avoid mixing effect. Each sampling trench (Fig. 3) had a depth of about 4.20 m. Table 1 gives descriptions of samples in more detail. Samples were collected in A and B trenches in December 2010 and in C, D and E trenches in August 2011 from the surface and different depths in each trench. All samples were first dried at room temperature and then sieved into size fractions of 40, 50, 70, 100, 140, 170, 200, 270, 325, 400 and −400 mesh in the mineral processing laboratory of the Sarcheshmeh copper mine. The samples were divided into two parts for mineralogical and geochemical analysis.

Mineralogical analysis

A mineralogical analysis was first conducted to qualitatively investigate the pyrite and chalcopyrite oxidation process at various depths of the tailings at the Central Laboratory of the Sarcheshmeh Copper Complex. The above 200-mesh sample fractions were fixed in epoxy resin and then prepared as standard polished sections in the mineral processing laboratory of the Sarcheshmeh copper mine. Optical microscopy was used to characterise oxidation process within the tailings materials.

X-ray diffraction analysis

All solid samples of tailings were analysed as bulk samples using X-ray diffraction (XRD). The samples were grounded with an agate mill and analysed immediately to prevent the alteration of minerals. XRD was qualitatively conducted by a Philips Xpert pro X-ray diffraction system at the Iran Mineral Processing Research Centre (IMPRC), Karaj, Iran.

X-ray fluorescence analysis

The chemical composition of the samples was also determined using a Philips Magix Pro X-ray Fluorescence (XRF) method at the Iran Mineral Processing Research

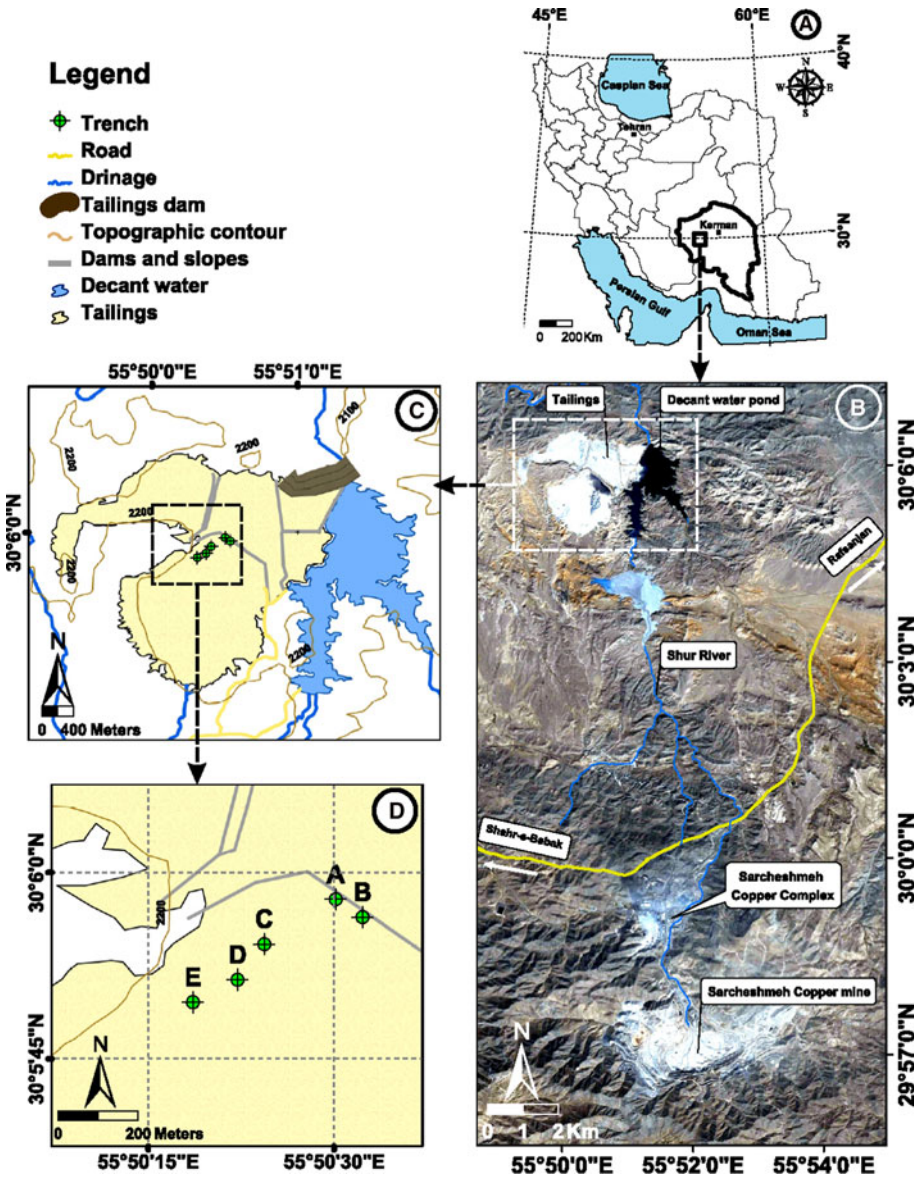

Fig. 1 Geographical location and simplified map of the study area and samples position on tailings

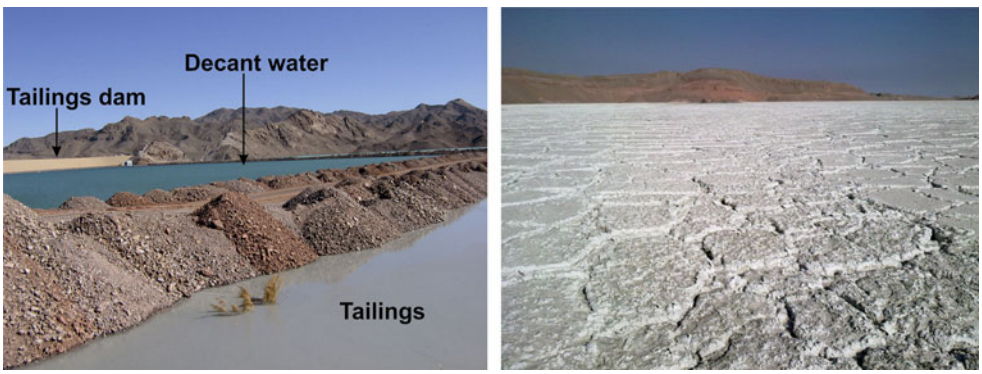

Fig. 2 Photographs indicating tailings at the Sarcheshmeh porphyry copper mine

Fig. 3 A trench excavated in the tailings site

Table 1 Depth samples descriptions of tailings materials

Trench	Height (m)	Sampling depth (m)	Number of samples in each trench
A	2,206	0, 0.3, 0.6, 0.9, 1.2, 1.5, 1.8, 2.10, 2.40, 2.70, 3, 3.30, 3.60, 3.90, 4.20	14
B	2,208	0, 0.3, 0.6, 0.9, 1.2, 1.5, 1.8, 2.10, 2.40, 2.70, 3, 3.30, 3.60, 3.90, 4.20	14
C	2,207	0, 0.3, 0.6, 0.9, 1.2, 1.5, 1.8, 2.10, 2.40, 2.70, 3, 3.30, 3.60, 3.90, 4.20	14
D	2,209	0, 0.3, 0.6, 0.9, 1.2, 1.5, 1.8, 2.10, 2.40, 2.70, 3, 3.30, 3.60, 3.90, 4.20	14
E	2,207	0, 0.3, 0.6, 0.9, 1.2, 1.5, 1.8, 2.10, 2.40, 2.70, 3, 3.30, 3.60, 3.90, 4.20	14
			Total 70

Centre (IMPRC), Karaj, Iran. The results are presented in "Results and discussion".

Geochemical analysis

The samples were first dried at 105 °C for about 8 h and then sieved. The less than 75 μm sample fractions were pulverised in an agate mill. About 20 g of each sample was systematically and statistically taken as the representative sample. The prepared samples were geochemically analysed for 61 bulk element concentrations by inductively coupled plasma mass spectrometry (ICP-MS) and inductively coupled plasma optical emission spectrometry (ICP-OES) in LabWest Minerals Analysis Pty Ltd., Australia with a detection limit varies between 0.05 and 2 ppm for most of the major and trace elements, except for Fe and S whose detection limit was 100 and 50 ppm respectively.

To prepare paste samples, 100 ml of distilled water was added to a 200 g sample. Hence, the water-to-soil ratio (W/S) was maintained approximately 1/2. The sample was then mixed with a spatula until a homogeneous paste readily slipping from the spatula was produced. The paste pH, electrical conductivity (EC) and major anions (HCO_3^-, CO_3^{2-}, Cl^- and SO_4^{2-}) concentration were analysed in the Molecule laboratory, Kerman, Iran. A HANA HI 9812 pH-EC meter was used to measure the pH of each paste sample. To perform measurement, the electrode of the instrument was inserted into the slurry and after swirling slightly, the paste pH was measured until a constant value was obtained. The EC of each sample was measured in a same manner as was conducted for pH.

The concentrations of anions including Cl^-, CO_3^{2-} and HCO_3^- were determined using titration.

To determine Cl^- concentration, 1 ml of potassium chromate (K_2CrO_4) was added in 50 ml of the sample. $AgNO_3$ was used for titration process. The experiment was ended as soon as a brick red colour was appeared. Carbonate and bicarbonate were measured by a titration process using HCl acid 0.02 N. Phenolphthalein ($C_2OH_{14}O_4$) and methyl orange were used as indicators.

The concentrations of SO_4^{2-}, NO_3^{2-} and NO_2^- were analysed by the use of a Spectrophotometer model

Spectronic 70 from Bausch and Lomb Company, USA. The sulphate was determined by adding about 5 ml of the sulphate stabiliser and 0.3 g of $BaCl_2$ to the prepared diluted solution before using the spectrophotometer. To measure nitrate, 1 ml of nitrate indicator and 10 ml of a concentrated sulphuric acid were added to 5 ml of the prepared sample. Before analysing by the spectrophotometer, it was held in a cold water bath for 5 min. Diluted solution.

Total reduced inorganic pyrite was determined using a standard method presented by ASTM (Gladfelter and Dickerhoof 1976). The less than 75 μm samples fractions were first prepared. Diluted Hydrochloric acid (HCl) was used to dissolve sulphate and oxide minerals. This acid had no effect on sulphide minerals. Diluted HNO_3 acid was then added to the solution system to dissolve sulphide minerals of the tailings samples. A 670 Shimadzu atomic absorption spectrometer (AAS) at the Faculty of Chemistry, Shahrood University of Technology was used to measure iron and copper concentrations in the solution. The concentrations of iron and copper were eventually used to determine pyrite and chalcopyrite contents remaining in the tailings particles based on their stoichiometric ratios.

Results and discussion

Analysis of the sample by XRD

The chemical and mineralogical constituents of tailings were determined using XRD method. Interpretation of XRD spectra of the samples show that they consisted of Quartz, SiO_2, approximately 32 %; Muscovite-illite, $KAl_2Si_3AlO_{10}(OH)_2$, 17 %; Chlorite, $(Mg,Fe)_6(Si,Al)_4O_{10}(OH)_8$, 15 %; Albite, $NaAlSi_3O_8$, 15 %; Orthoclase, $KAlSi_3O_8$, 10 % and Pyrite, FeS_2, 8 % as the main mineral phases (Fig. 4).

Analysis of the sample by XRF

The results show that the sample analysed by XRF method consisted of SiO_2: 62.4 wt %, Al_2O_3: 16.7 wt %, SO_3: 6 wt %, K_2O: 5.3 wt %, MgO: 2.95 wt % and Na_2O: 2.9 wt %. It is obvious that SiO_2 and Al_2O_3 are the major oxide phases of the tailings at the Sarcheshmeh mine.

Mineralogical data

Pyrite and chalcopyrite were the main primary sulphide minerals that occurred as variable size fractions. They are fine or coarse grained (5–200 micron) in polished sections of tailings samples (Figs. 5, 6). Pyrite is almost cubic. The polished sections show depletion of pyrite and chalcopyrite in the oxidised zone. They are present in the unoxidised zone of the tailings. Oxygen is readily available at the tailings surface. So, the rate of pyrite oxidation is very high. The polished section from the tailings surface (Fig. 5a) shows no pyrite. However, some chalcopyrite grains are seen from the tailings surface sample (Fig. 6a). Due to the rapid reduction in oxygen diffusion with depth, the sulphide minerals' oxidation decreased. Less oxidised pyrite and chalcopyrite grains were observed at a depth of 1 m (Figs. 5b, 6b). Totally unoxidised pyrite and chalcopyrite minerals can be easily seen in the polished sections of a depth of 4 m (Figs. 5c, 6c), where no oxygen is available to oxidise them (modified after Jannesar Malakooti et al. 2012).

Geochemical data

Pyrite oxidation process

Pyrite oxidation is the major source of AMD in mine spoils and tailings. Therefore, it is very important to investigate this process in the tailings of the Sarcheshmeh copper

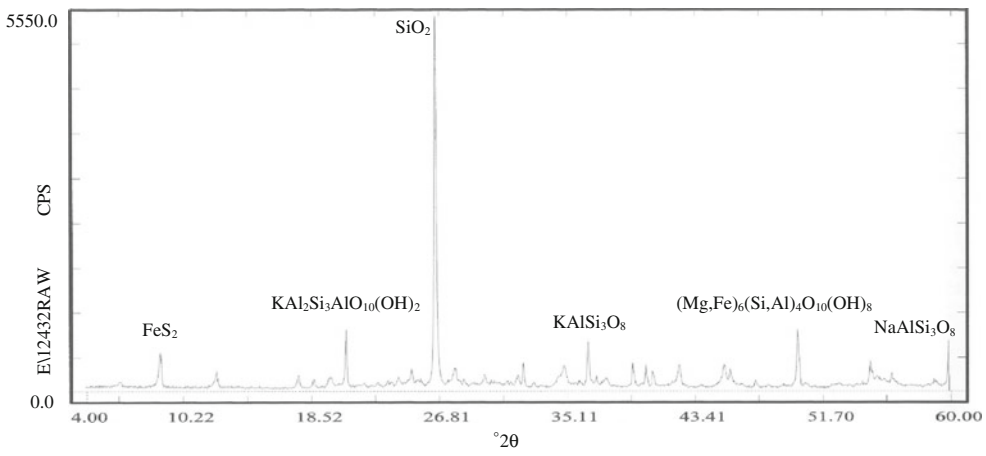

Fig. 4 XRD pattern for a sample from the Sarcheshmeh tailings

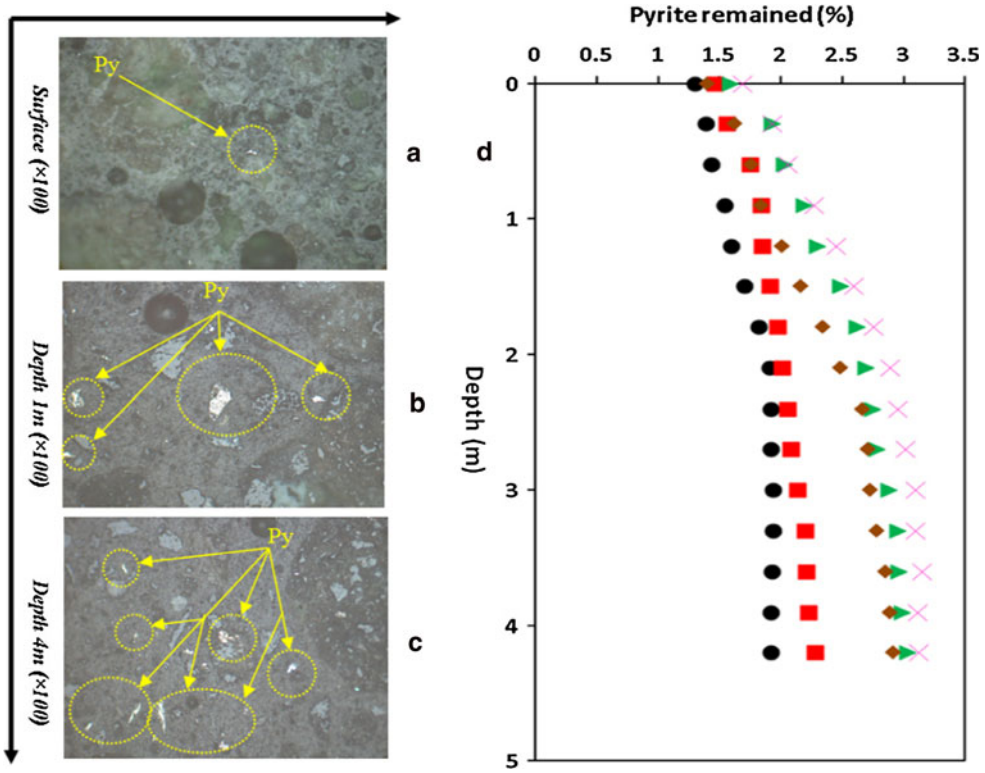

Fig. 5 Polished sections of the profile D solid samples in the tailings dam; representing pyrite reduction in the samples at shallower depths of the tailings. **a** The tailings surface, **b** at a depth of 1 m, **c** at a depth of 4 m, **d** pyrite content remained (wt %) versus depth. *Py* Pyrite, *filled circles* indicate A, *filled square* show B, *filled triangles* indicate C, *filled diamonds* indicate D and *crossed line* indicate E profiles

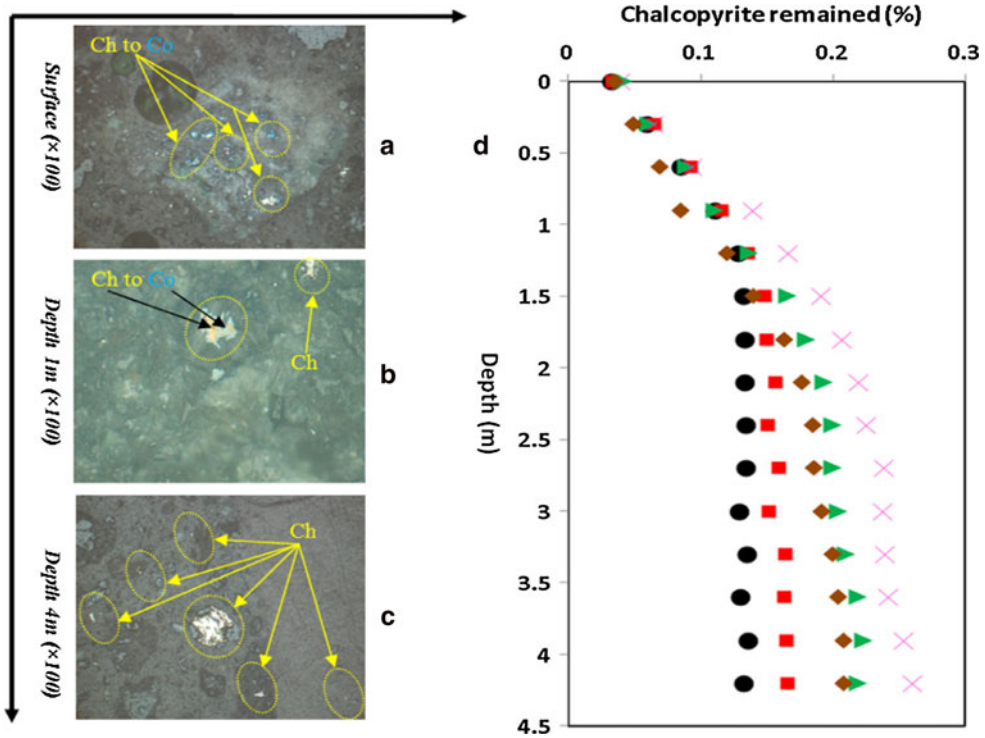

Fig. 6 Polished sections of profile D solid samples in the tailings dam; showing chalcopyrite depletion in the samples at shallower depths and its replacement with covellite of the tailings samples. **a** The dam surface, **b** at a depth of 1 m, **c** at a depth of 4 m, **d** chalcopyrite content remained (wt %) versus depth. *Ch* Chalcopyrite and *Co* Covellite. *Filled circles* indicate A, *filled square* show B, *filled triangles* indicate C, *filled diamonds* indicate D and *crossed line* indicate E profiles

mine. Recent studies reveal that pyrite oxidation is very complex because many chemical, biological, and electrochemical reactions are involved (Evangelou and Zhang 1994; Evangelou 1995). Four methods comprising inorganic/biochemical reaction approach, electrochemical reaction approach, reaction kinetics approach and computer simulation approach have been developed to investigate pyrite oxidation process (Evangelou 1995). In this paper, we apply geochemical and mineralogical studies to consider pyrite and chalcopyrite oxidation.

Determining the remaining pyrite and chalcopyrite can provide useful information to understand the reactivity of the fine grains in tailings (Shahhoseiny et al. 2013). The fraction of pyrite remaining ranged from (1.403–1.928 wt %), (1.571–2.286 wt %), (1.936–3.04 wt %), (1.938–3.134 wt %) and (1.629–2.914 wt %) in A, B, C, D and E profiles, respectively (Table 2). The content of chalcopyrite remaining ranged from (0.06–0.133 wt %), (0.065–0.166 wt %), (0.061–0.219 wt %), (0.065–0.261 wt %) and (0.049–0.208 wt %) in A, B, C, D and E profiles, respectively (Table 3). There is almost a considerable difference between pyrite remaining at tailings surface and greater depth of each profile; demonstrating that high amount of pyrite oxidised in the tailings materials.

The pyrite oxidation process is more extreme in profile D than the profiles A, B, C and E due to the fact that oxygen can diffuse more easily through the relatively coarse-grained tailings particles containing pyrite in this profile. Pyrite oxidation is more obvious at the upper 1.2, 1.2, 1.8, 2.1 and 1.5 m of the profiles A, B, C, D and E in tailings, respectively (Fig. 5). It decreased steadily at lower depths, up to a depth of about 1.5 m, in the five profiles. Below this depth, oxidation process gradually decreased, and it entirely stopped at an approximate depth of 3.5 m.

Chalcopyrite oxidation

The oxidation of chalcopyrite is expressed by the following reaction:

$$CuFeS_2 + 4O_2 \Rightarrow 2Cu^{2+} + Fe^{2+} + SO_4^{2-} \quad (5)$$

Reaction 5 produces no acid. However, the combination of ferrous iron oxidation and ferrihydrate hydrolysis will produce acid according to the following reaction:

$$2CuFeS_2 + \frac{17}{2}O_2 + 5H_2O \Rightarrow 2Cu^{2+} + 2Fe(OH)_3 + 4SO_4^{2-} + 4H^+ \quad (6)$$

.

Chalcopyrite is recognised as one of the most resistant sulphides to participate in oxidation reaction (Plumlee 1999). According to Rimstidt et al. (1994), chalcopyrite oxidation rate increases with an increase in ferric iron concentration, but with an oxidation rate of 1–2 orders of magnitude less than pyrite.

Below the water-table, with increasingly reducing conditions, chalcopyrite is replaced by covellite, leading to secondary Cu enrichments (Jang and Wadsworth 1994). This is mainly a pH dependent process, because the pH controls the mobility of Cu. Cu is mobile below a pH of 5.5 only. This replacement can occur under this pH condition.

The high resistance of chalcopyrite to weathering process depends on the fact that the grains are often encapsulated in silicate grains in tailings materials, and thereby may escape from the dissolution processes (Jambor 1994).

Chalcopyrite oxidation in the presence of ferric iron under acidic conditions can be expressed as:

$$CuFeS_2 + 4Fe^{3+} \Rightarrow 5Fe^{2+} + Cu^{2+} + 2S^0 \quad (7)$$

.

Hiroyoshi et al. (1997) observed the oxygen consumption, sulphur formation, total iron, and Fe(II)

Table 2 Pyrite content remaining in depth solid samples of tailings

Location A			Location B			Location C			Location D			Location E		
Depth (cm)	Samples	FeS_2 (wt %)	Depth (cm)	Samples	FeS_2 (wt %)	Depth (cm)	Samples	FeS_2 (wt %)	Depth (cm)	Samples	FeS_2 (wt %)	Depth (cm)	Samples	FeS_2 (wt %)
30	A_1	1.403	30	B_1	1.571	30	C_1	1.936	30	D_1	1.938	30	E_1	1.629
60	A_2	1.442	60	B_2	1.758	60	C_2	2.041	60	D_2	2.067	60	E_2	1.762
90	A_3	1.549	90	B_3	1.845	90	C_3	2.20	90	D_3	2.283	90	E_3	1.841
120	A_4	1.606	120	B_4	1.861	120	C_4	2.305	120	D_4	2.463	120	E_4	2.013
150	A_5	1.715	150	B_5	1.825	150	C_5	2.497	150	D_5	2.606	150	E_5	2.163
180	A_6	1.830	180	B_6	1.988	180	C_6	2.63	180	D_6	2.767	180	E_6	2.343
210	A_7	1.920	210	B_7	2.02	210	C_7	2.702	210	D_7	2.895	210	E_7	2.483
240	A_8	1.930	240	B_8	2.06	240	C_8	2.758	240	D_8	2.96	240	E_8	2.663
270	A_9	1.930	270	B_9	2.09	270	C_9	2.79	270	D_9	3.025	270	E_9	2.708
300	A_{10}	1.950	300	B_{10}	2.146	300	C_{10}	2.89	300	D_{10}	3.106	300	E_{10}	2.727
330	A_{11}	1.945	330	B_{11}	2.209	330	C_{11}	2.965	330	D_{11}	3.105	330	E_{11}	2.780
360	A_{12}	1.936	360	B_{12}	2.221	360	C_{12}	2.97	360	D_{12}	3.159	360	E_{12}	2.858
390	A_{13}	1.927	390	B_{13}	2.236	390	C_{13}	3.00	390	D_{13}	3.124	390	E_{13}	2.893
420	A_{14}	1.928	420	B_{14}	2.286	420	C_{14}	3.04	420	D_{14}	3.134	420	E_{14}	2.914

Table 3 Chalcopyrite content remaining in depth solid samples of tailings

Location A			Location B			Location C			Location D			Location E		
Depth (cm)	Samples	$CuFeS_2$ (wt %)	Depth (cm)	Samples	$CuFeS_2$ (wt %)	Depth (cm)	Samples	$CuFeS_2$ (wt %)	Depth (cm)	Samples	$CuFeS_2$ (wt %)	Depth (cm)	Samples	$CuFeS_2$ (wt %)
30	A_1	0.060	30	B_1	0.065	30	C_1	0.061	30	D_1	0.065	30	E_1	0.049
60	A_2	0.086	60	B_2	0.092	60	C_2	0.089	60	D_2	0.0094	60	E_2	0.069
90	A_3	0.112	90	B_3	0.116	90	C_3	0.111	90	D_3	0.140	90	E_3	0.085
120	A_4	0.129	120	B_4	0.136	120	C_4	0.137	120	D_4	0.167	120	E_4	0.120
150	A_5	0.133	150	B_5	0.148	150	C_5	0.166	150	D_5	0.192	150	E_5	0.140
180	A_6	0.134	180	B_6	0.150	180	C_6	0.180	180	D_6	0.207	180	E_6	0.163
210	A_7	0.134	210	B_7	0.157	210	C_7	0.193	210	D_7	0.220	210	E_7	0.177
240	A_8	0.135	240	B_8	0.151	240	C_8	0.200	240	D_8	0.226	240	E_8	0.185
270	A_9	0.135	270	B_9	0.159	270	C_9	0.200	270	D_9	0.239	270	E_9	0.186
300	A_{10}	0.130	300	B_{10}	0.152	300	C_{10}	0.204	300	D_{10}	0.238	300	E_{10}	0.192
330	A_{11}	0.136	330	B_{11}	0.164	330	C_{11}	0.210	330	D_{11}	0.240	330	E_{11}	0.200
360	A_{12}	0.131	360	B_{12}	0.163	360	C_{12}	0.219	360	D_{12}	0.242	360	E_{12}	0.204
390	A_{13}	0.137	390	B_{13}	0.165	390	C_{13}	0.223	390	D_{13}	0.254	390	E_{13}	0.208
420	A_{14}	0.133	420	B_{14}	0.166	420	C_{14}	0.219	420	D_{14}	0.261	420	E_{14}	0.208

concentrations at different pH values during the oxidation of chalcopyrite. Based on the oxidation products formed, they concluded that ferrous ions catalysed the oxidation by dissolved oxygen in an acidic medium:

$$CuFeS_2 + 4H^+ + O_2 \Rightarrow Cu^{2+} + Fe^{2+} + 2S^0 + 2H_2O \quad (8)$$

.

The dissolution of chalcopyrite can be also affected strongly by galvanic effects. The presence of pyrite or molybdenite together with chalcopyrite can accelerate kinetics of chalcopyrite dissolution (Dutrizac and MacDonald 1973), whereas the presence of iron-rich sphalerite and galena can decrease the dissolution rate (Blowes et al. 2003).

Similar to pyrite oxidation, the chalcopyrite oxidation process is more intense in the profile D than four others because of the same reason discussed above for pyrite oxidation. The geochemical analysis of the samples for chalcopyrite remaining shows oxidation process at the upper 1, 1.2, 1.5, 2.0 and 1.8 m of the profiles A, B, C, D and E in tailings, respectively (Fig. 6). The chalcopyrite oxidation decreased sharply at shallower depths, up to a depth of 1.5 m in the all the profiles of tailings (Fig. 6) due to a rapid reduction in oxygen diffusion through the tailings materials. Below this depth, up to an approximate depth of about 3.5 m, it decreased again with a gradual rate. Below 3.5 m depth, the oxidation process completely ceased.

pH and major anions

The pH and electrical conductivity values, sulphate, bicarbonate, carbonate and chloride concentrations in tailings solid samples are given in Table 4. Variations of pH and SO_4^{2-}, Cl^-, HCO_3^-, NO_2^- and NO_3^{2-} concentrations with depth in tailings solid samples from the five profiles are shown in Fig. 7.

The SO_4^{2-} concentration is a main product of pyrite oxidation. The maximum concentration for SO_4^{2-} of 1,300, 1,170, 1,852.4, 1,960.9 and 837 mg/L was observed at a depth of 0.9 m in the profiles A, B, C, D and E, respectively. In the zone between 0.9 and 1.5 m, the sulphate decreased linearly. Below 1.5 m, it remains constant with depth. Sulphate concentration produced by the pyrite oxidation decreases more quickly in the profile D, most probably due to a rapid migration of water through the profile D. This may reduce the possibility of sulphate precipitation in solid phase at the upper layers of the tailings materials.

pH is low in surface layers of tailings where the concentration of oxygen is high and sulphide minerals' oxidation is significant. The lowest pH values 2.9, 3, 3, 2.7 and 3.5 were measured at a depth of 0.3 m in the profiles A, B, C, D and E, respectively. It increased steadily up to a depth of 2.1 m. Below this depth, it almost remains constant. The acid liberated from sulphide minerals' oxidation has completely depleted carbonate minerals in the tailings vertical profiles. Hence, a zero concentration was measured for CO_3^{2-} ion in the five profiles (Table 4). HCO_3^- varies from 0 to 30, 1 to 17, 0 to 52.5, 0 to 52.5 and 0 to 52.5 mg/L in the profiles A, B, C, D, E and F, respectively. The maximum concentration of HCO_3^-, 30, 17, 52.5, 52.5 and 54.5 mg/L was observed at depths 2.1, 1.8, 1.5, 2.1 and 3.9 m in the profiles A, B, C, D and E, respectively.

The maximum values of electrical conductivity (EC) 12×10^3, 12.5×10^3, 14×10^3, 15×10^3 and 13×10^3 μS/cm were detected at depths 0.9, 0.9, 0.9, 0.9

Table 4 Geochemical analyses of tailings samples for pH, EC and major anions at the Sarcheshmeh copper mine (all concentrations are in mg/L)

Samples no./depth (m)	Parameters						NO_2^-	NO_3^{2-}
	pH	EC	SO_4^{2-}	CO_3^{2-}	HCO_3^-	Cl^-		
A30/0.3	2.9	>12,000	844	0	0	42.4	19.8	4.3
A60/0.6	3.1	>12,000	1,150	0	0	40.7	11.0	3.2
A90/0.9	4.5	>12,000	1,300	0	0	34.1	12.2	1.8
A120/1.2	4.7	>12,000	928	0	0	30.7	10.2	3.1
A150/1.5	5.6	>12,000	901	0	20	19.0	14.9	3.9
A180/1.8	6.7	>12,000	870	0	25	22.4	16.9	4.3
A210/2.1	7.0	>12,000	863	0	30	19.0	14.3	5.2
A240/2.4	7.8	>12,000	808	0	25	17.1	14.7	5.5
A270/2.7	7.3	>12,000	850	0	30	17.2	20.3	7.2
A300/3.0	7.6	>12,000	835	0	22	15.5	10.6	7.6
A330/3.3	7.8	>12,000	800	0	28	15.5	6.9	6.5
A360/3.6	8.2	>12,000	915	0	26	12.1	6.7	6.3
A390/3.9	7.9	>12,000	905	0	25	13.8	6.3	5.9
A420/4.2	8.3	>12,000	910	0	23	20.7	6.5	6.1
B30/0.3	3.0	>12,000	538	0	12	34.1	14.8	9.7
B60/0.6	3.5	>12,000	1,000	0	4	31.1	5.5	5.0
B90/0.9	4.0	>12,000	1,170	0	3	28.4	5.0	4.7
B120/1.2	5.0	>12,000	570	0	2	26.4	10.9	4.4
B150/1.5	6.6	>12,000	600	0	1	20.4	10.2	2.7
B180/1.8	6.9	>12,000	607	0	17	24.4	9.9	2.9
B210/2.1	7.2	>12,000	653	0	13	23.7	20.8	4.3
B240/2.4	7.1	>12,000	634	0	12	25.9	18.1	4.4
B270/2.7	7.6	>12,000	600	0	10	25.9	15.0	5.6
B300/3.0	8.1	>12,000	667	0	15	24.1	15.2	5.9
B330/3.3	8.3	>12,000	670	0	10	24.1	14.9	5.4
B360/3.6	8.2	>12,000	634	0	13	24.1	21.2	4.7
B390/3.9	7.9	>12,000	701	0	17	20.7	21.7	6.7
B420/4.2	8.2	>12,000	730	0	12	25.9	20.0	6.5
C30/0.3	3.0	>12,000	1,053.8	0	0	54.95	0.75	14.63
C60/0.6	3.2	>12,000	1,342.2	0	0	46.65	0.75	12.88
C90/0.9	3.8	>12,000	1,852.4	0	0	45.21	0.75	6.5
C120/1.2	6.3	>12,000	937.7	0	21	40.69	0.75	4.63
C150/1.5	6.8	>12,000	380.9	0	52.5	27.13	0.1	0
C180/1.8	7.2	>12,000	314.1	0	47.2	20.61	0.75	0
C210/2.1	8.0	>12,000	309.2	0	47.2	22.61	0.75	0
C240/2.4	7.7	>12,000	358.9	0	42	27.13	0.75	0
C270/2.7	7.8	>12,000	315.4	0	42	22.61	0.75	0
C300/3.0	8.2	>12,000	333.9	0	47.2	22.61	0.1	0
C330/3.3	8.1	>12,000	309.2	0	42	22.61	0.1	0
C360/3.6	8.0	>12,000	339.6	0	47.2	22.61	0.075	0
C390/3.9	7.9	>12,000	355.4	0	47.2	22.61	0.075	0
C420/4.2	8.3	>12,000	325.6	0	36.7	22.61	0.075	0
D30/0.3	4.8	>12,000	1,500	0	15.7	82.21	0.1	22.63
D60/0.6	3.9	>12,000	1,708.3	0	10.5	67.82	0.08	9.75
D90/0.9	5.2	>12,000	1,960.9	0	0	52.21	0.075	4.63
D120/1.2	6.6	>12,000	1,165.6	0	10.5	45.21	0.079	1.38

Table 4 continued

Samples no./depth (m)	Parameters						NO_2^-	NO_3^{2-}
	pH	EC	SO_4^{2-}	CO_3^{2-}	HCO_3^-	Cl^-		
D150/1.5	7.1	>12,000	637.8	0	47.2	45.21	0	0.75
D180/1.8	7.6	>12,000	535.1	0	42	21.61	0.05	0
D210/2.1	7.0	>12,000	516.3	0	52.5	22.61	0.075	0
D240/2.4	7.4	>12,000	449	0	52.5	22.61	0.075	0
D270/2.7	8.0	>12,000	398.8	0	37	22.61	0.1	0
D300/3.0	7.8	>12,000	383.3	0	35	22.61	0.1	0
D330/3.3	8.1	>12,000	375.3	0	40	22.61	0.075	0
D360/3.6	7.9	>12,000	340.1	0	47	22.61	0.075	0
D390/3.9	7.8	>12,000	384.9	0	48	22.61	0.175	0
D420/4.2	7.8	>12,000	391.4	0	50	22.61	0.075	0
E30/0.3	4.2	>12,000	321.9	0	52.5	80.82	0.075	7.13
E60/0.6	3.8	>12,000	589.5	0	0	78.72	0.15	0
E90/0.9	3.0	>12,000	837	0	0	78.78	0.075	0
E120/1.2	6.2	>12,000	622.5	0	42	73.99	0.075	0
E150/1.5	7.4	>12,000	444.7	0	52.5	67.82	0.075	0
E180/1.8	8.1	>12,000	351.4	0	42	28.61	0.075	0
E210/2.1	8.6	>12,000	365.2	0	42	25.76	0.05	0
E240/2.4	8.4	>12,000	309.2	0	47.2	22.61	0.075	0
E270/2.7	8.4	>12,000	337.2	0	42	18.09	0.075	0
E300/3.0	8.3	>12,000	351.4	0	52.5	18.09	0.15	0
E330/3.3	8.3	>12,000	358.9	0	47.2	18.09	0.075	0
E360/3.6	7.9	>12,000	366.8	0	46.2	18.09	0.075	0
E390/3.9	8.1	>12,000	314	0	52.5	18.09	0.075	0
E420/4.2	8.0	>12,000	371.6	0	52.5	22.61	0.1	0

and 3.5 m in the profiles A, B, C, D and E. These values were directly measured at the site during sampling process. EC decreased with depth in the profiles A, B and E but it increased versus depth in the profiles C and D.

Major and trace elements

Sulphide minerals' oxidation and AMD generation often cause the concentrations of heavy metals to be elevated. An investigation of the geochemistry of trace elements is important for comprehensive assessment of the potential environmental impacts of mine drainages. For this reason, a geochemical analysis was carried out to measure the concentrations of major (Table 5) and trace elements (Table 6) in tailings materials. These tables give the maximum, minimum and mean concentrations for major, rare earth and trace elements of A, B, C, D and E profiles of tailings.

One of the main objectives of this research was to identify the mobility of trace elements in the copper mine tailings. Major and trace elements concentrations vary significantly in the five profiles of tailings. Total S concentrations ranged from 20,620 to 30,218, from 18,551 to 28,525, from 16,200 to 27,300, from 6,550 to 26,700 and from 10,100 to 20,000 mg/L in A, B, C, D and E profiles, respectively. In addition, Fe concentrations range from 30,800 to 53,100, from 27,000 to 54,600, from 29,500 to 47,100, from 21,500 to 56,800 and from 23,700 to 42,100 in A, B, C, D and E profiles, respectively. Major elements concentrations strongly reflect the mineralogy of the tailings materials throughout the vertical profiles. The Fe and S contents indicate the presence of sulphide minerals in particular pyrite with tailings particles.

SiO_2 (30–70 wt %), Al_2O_3 (13–18 wt %) and Fe_2O_3 (2–5 wt %) occurred as the major gangue minerals in the mine tailings. The aluminium (6–9 wt %) content most probably indicates the presence of aluminosilicate minerals in the tailings materials. The tailings are characterised by considerable amounts of trace elements: Mn (285–1,090 ppm), Ba (311–792.6 ppm), Sr (110–258.1 ppm), Zn (112–243.2 ppm), Cu (0.1–0.242 %), Pb (30.4–54.4 ppm), Li (5.4–13.2 ppm), Ni (18–43 ppm), Mo (51.1–198.6 ppm), Rb (71–156.3 ppm) and V (76–196 ppm). Fe, Al, S, Mn, Ba, Sr, Zn and Cu were the most abundant major and trace elements measured in the tailings materials (Fig. 8).

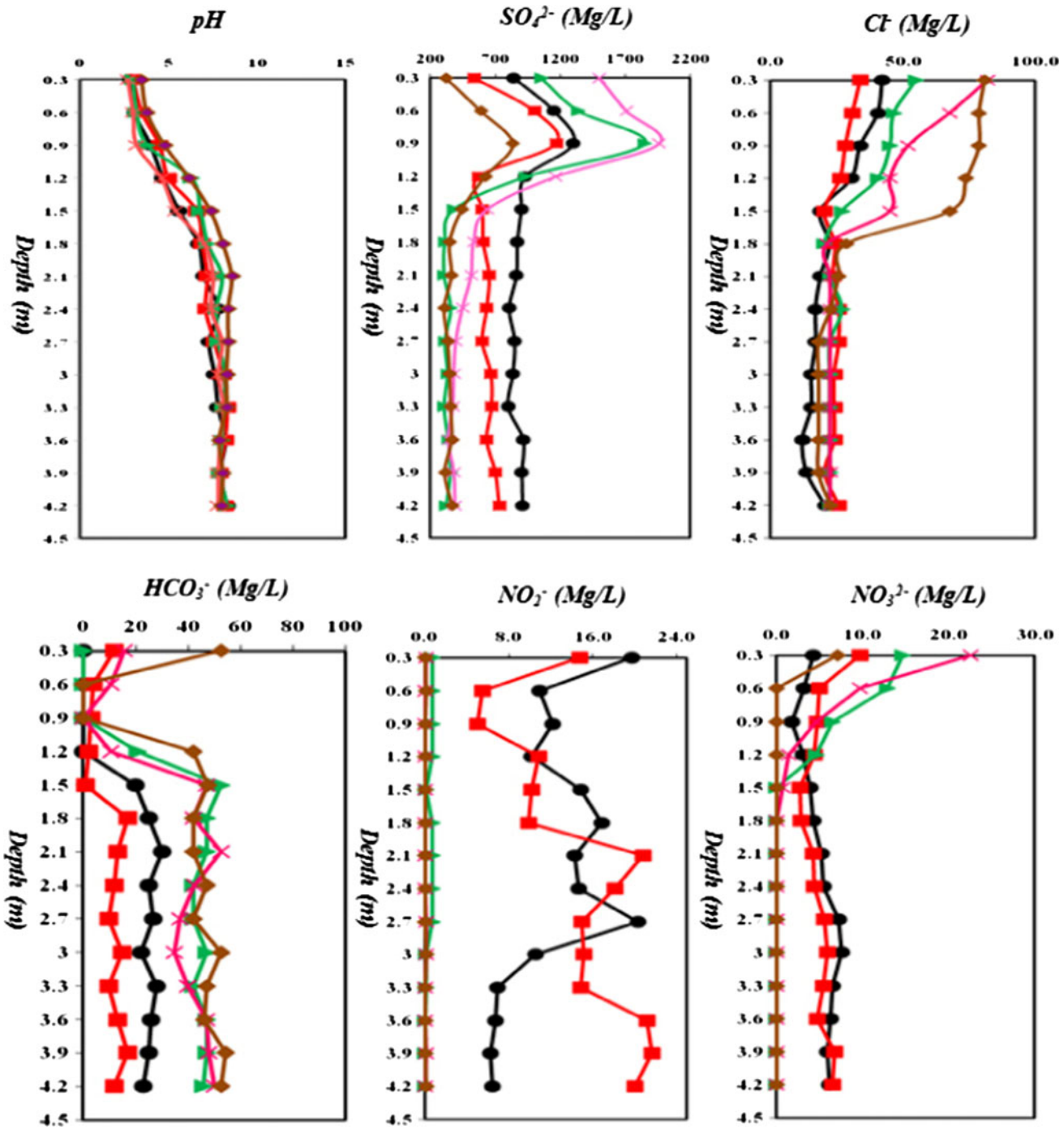

Fig. 7 Vertical depth profiles of pH and major anions (SO_4^{-2}, Cl^-, HCO_3^-, NO_2^- and NO_3^{2-}) variations for trenches A, B, C, D and E of tailings at the Sarcheshmeh copper mine, *filled circles* indicate A, *filled square* show B, *filled triangles* indicate C, *filled diamonds* indicate D and *crossed line* indicate E profiles

Formation of secondary minerals

Gypsum, Mg-sulphates and trace element sulphates are the major phases at surface layers of the tailings materials. These newly formed minerals tend to precipitate in the oversaturated pore solutions. The dominant metal sulphates are Fe-sulphate ($Fe_2(SO_4)_3$), Cu-sulphate ($CuSO_4$), followed by Mg-sulphate ($MgSO_4$). Furthermore, Zn-sulphate ($ZnSO_4$), Na-sulphate (Na_2SO_4) and Mn-sulphate ($MnSO_4$) are often found at some sites.

According to Fig. 9, the SO_4^{2-} concentration exhibits no correlation with Ca ($r = 0.037$) in the profile A and a

Table 5 Concentrations of major elements and iron species (Fe^{2+} and Fe^{3+}) (μg/g) in the Sarcheshmeh copper mine tailings

Samples	Al	Ca	Fe	Fe^{2+}	Fe^{3+}	K	Mg	Na	P	S	Ti	Ce	La
Location A													
A30	85,257	11,041	53,100	16,100	37,000	34,607	18,347	11,270	850	25,059	2,005	37.39	20.83
A60	85,212	6,421	49,000	11,900	37,100	36,758	16,376	10,487	825	29,479	1,841	37.79	21.01
A90	82,299	5,857	37,800	11,500	36,500	36,166	14,088	9,857	704	29,457	1,784	41.6	23.34
A120	75,676	5,197	30,900	10,900	20,000	37,295	9,336	8,125	665	21,658	1,494	36.35	20.4
A150	74,905	4,338	30,800	8,700	22,100	35,668	8,507	8,729	565	20,870	1,323	31.17	19.25
A180	83,324	5,034	30,200	5,400	24,800	36,070	8,952	8,608	766	20,620	1,252	35.18	19.76
A210	80,134	5,500	32,700	5,400	27,300	35,535	8,859	8,541	720	21,260	1,128	34.16	19.53
A240	80,083	5,298	33,100	21,100	12,000	36,120	8,291	7,055	671	22,914	1,097	36.53	20.82
A270	81,371	5,590	34,200	24,500	9,700	36,000	9,120	7,435	729	23,752	1,200	32.72	19.45
A300	80,067	5,899	34,000	24,200	9,800	37,639	8,928	8,892	778	23,603	1,268	33.11	19.68
A330	78,473	5,780	35,600	24,700	10,900	38,195	8,901	9,451	711	24,281	1,171	39.47	22.92
A360	85,062	6,335	35,000	26,300	8,700	33,819	9,229	9,004	829	25,743	1,111	37.89	22.01
A390	82,926	6,137	36,300	29,800	6,500	32,646	9,340	9,391	713	28,768	1,208	42.15	23.97
A420	79,578	6,605	37,100	29,100	8,000	33,915	8,863	10,501	662	30,218	1,279	37.95	22.01
Min	74,905	4,338	30,200	5,400	6,500	32,646	8,291	7,055	565	20,620	1,111	31.17	19.25
Mean	80,618.13	5,958	36,000	17,828.6	19,314.3	35,538.6	10,361.9	8,960	716.7	24,553.5	1,351.5	36.3	20.95
Max	85,257	11,041	53,100	29,800	37,100	38,195	18,347	11,270	850	30,218	2,005	42.15	23.97
Location B													
B30	89,998	8,974	54,600	16,300	38,300	36,432	18,754	10,309	851	23,094	2,465	37.75	21.5
B60	81,809	7,737	44,600	15,200	29,400	34,201	15,138	7,751	758	35,370	1,983	33.95	18.54
B90	84,042	6,600	41,900	14,900	27,000	35,307	14,884	7,845	782	28,525	2,000	36.13	20.71
B120	82,052	6,491	34,700	8,300	26,400	36,501	13,929	8,917	749	23,115	1,969	40.15	22.64
B150	76,154	5,851	27,600	7,600	20,000	37,898	9,509	9,752	661	18,551	1,778	39.53	22.53
B180	73,080	4,908	27,000	6,400	20,600	34,018	8,765	9,322	608	20,572	1,411	37.03	20.77
B210	76,787	5,176	28,700	6,500	22,200	34,248	8,801	9,724	691	21,626	1,311	32.67	18.33
B240	73,184	5,294	29,400	24,400	5,400	34,111	8,679	8,967	705	20,116	1,265	31.79	18.08
B270	76,877	5,636	29,700	25,400	4,300	35,425	8,407	8,828	668	20,579	1,275	36.14	20.65
B300	75,662	5,125	29,400	24,000	5,400	35,829	7,161	8,661	648	21,091	1,275	37.19	20.96
B330	72,366	4,935	30,200	26,900	3,300	33,832	7,863	8,204	662	22,504	1,242	30.12	22.49
B360	73,266	4,731	30,000	27,800	2,200	35,525	7,817	8,227	669	20,589	1,264	33.94	23.55
B390	77,591	4,864	31,200	24,700	6,500	37,556	8,358	8,578	669	23,289	1,213	44.08	25.47
B420	82,080	5,794	31,800	22,000	9,800	34,806	9,030	9,214	852	24,858	1,252	41.53	23.52
Min	72,366	4,731	27,000	6,400	2,200	33,832	7,161	7,751	661	18,551	1,213	30.12	18.08
Mean	77,820.9	5,789.8	33,186.7	17,885.7	15,771.4	35,301.4	10,283.7	8,803.3	708.9	22,828.7	1,527.7	36.14	21.18
Max	89,998	8,974	54,600	27,800	38,300	37,898	18,725	10,309	851	35,370	2,465	44.08	25.47
Location C													
C30	71,400	4,220	47,100	17,100	30,000	31,300	9,370	11,900	663	16,800	1,580	28.6	15.7
C60	57,400	4,130	42,000	14,000	28,000	30,000	6,230	10,400	632	27,300	1,480	22.9	12.7
C90	64,100	4,440	38,800	15,800	23,000	32,700	7,360	7,830	552	18,400	1,570	27.6	14.8
C120	61,600	4,080	34,000	9,000	25,000	30,900	7,250	7,800	573	17,900	1,460	24.6	13
C150	54,900	5,810	30,000	10,000	20,000	28,000	7,440	7,020	550	20,100	1,440	22.7	12.3
C180	62,400	5,670	31,300	12,300	19,000	30,700	7,920	7,430	636	19,600	1,490	22.2	13.6
C210	63,600	5,710	31,000	20,000	11,000	31,000	7,780	7,420	620	20,600	1,430	26.6	14.6
C240	69,600	4,380	31,000	23,000	8,000	29,400	7,700	7,550	671	21,000	1,510	31.8	17.2
C270	71,300	4,360	30,700	25,000	5,700	34,200	8,940	7,310	664	21,000	1,640	27.5	16.6
C300	74,400	4,980	31,800	25,900	5,900	35,500	7,940	7,980	761	16,200	1,560	34.3	18.6
C330	75,200	5,570	31,000	27,000	4,000	36,400	8,210	8,980	746	16,000	1,650	38.1	20.9

Table 5 continued

Samples	Al	Ca	Fe	Fe^{2+}	Fe^{3+}	K	Mg	Na	P	S	Ti	Ce	La
C360	72,100	5,140	30,000	26,000	4,000	30,800	8,460	8,640	777	16,500	1,730	31.1	21
C390	68,700	5,030	29,700	27,000	2,700	31,500	9,030	8,300	746	17,000	1,900	31.3	20.8
C420	69,900	5,670	29,500	28,000	1,500	29,200	9,640	9,490	783	18,600	1,910	30.3	20.3
Min	54,900	4,130	29,500	9,000	1,500	28,000	6,230	7,020	620	16,000	1,430	22.2	12.3
Mean	66,100	4,888	33,160	20,007.1	13,414.3	31,306.7	7,966.7	8,338	666.3	18,866.7	1,585.3	28.12	16.3
Max	71,400	5,810	47,100	28,000	30,000	32,700	9,640	11,900	783	27,300	1,900	38.1	20.9
Location D													
D30	67,400	6,740	56,800	17,800	39,000	24,800	14,500	10,800	622	16,100	2,480	32.4	17.9
D60	65,600	6,160	44,100	12,100	32,000	25,700	10,600	6,650	562	26,700	2,020	31.4	16.8
D90	63,300	5,140	36,700	16,700	30,000	25,300	9,400	6,910	567	13,800	1,700	32.5	17.7
D120	65,200	4,170	30,300	10,300	20,000	24,700	7,410	6,650	467	11,030	1,600	37.7	20.9
D150	58,800	3,160	26,800	18,800	8,000	23,700	6,580	6,590	379	12,890	1,175	32.2	17.5
D180	54,100	3,220	25,700	12,800	12,900	25,500	6,600	5,190	442	13,200	1,154	28.4	15.4
D210	52,600	2,820	24,300	8,000	16,300	24,500	7,360	5,620	477	14,300	1,126	23.1	16.1
D240	53,900	3,450	23,700	18,700	5,000	23,600	7,150	5,330	513	13,600	1,116	24	16.4
D270	59,000	3,660	23,200	17,500	5,700	24,300	7,420	5,090	458	12,000	1,164	38.3	21
D300	58,900	3,050	21,800	17,500	4,300	23,100	5,190	6,680	471	7,020	1,196	37.3	20.4
D330	61,300	3,770	22,500	14,500	8,000	23,900	5,450	7,320	546	7,350	1,242	39.2	21
D360	63,700	3,920	22,400	18,000	4,400	23,600	5,910	7,300	572	7,880	1,250	45.2	24.6
D390	64,000	3,880	22,800	19,000	3,800	24,700	6,980	7,980	520	6,550	1,228	41.6	23
D420	60,800	3,750	21,500	18,700	2,800	22,500	6,810	8,090	540	8,530	1,190	41.3	22.9
Min	52,600	2,820	21,500	8,000	2,800	22,500	5,190	5,090	379	6,550	2,020	23.1	15.4
Mean	60,080	3,980.7	28,273.4	15,742.8	13,728.6	24,160	7,503.4	6,752.7	501	11,833.4	1,444	33.8	19.13
Max	67,400	6,740	56,800	19,000	39,000	25,700	14,500	10,800	622	26,700	2,480	45.2	24.6
Location E													
E30	59,000	5,340	42,100	10,100	32,000	22,100	11,500	9,580	499	10,100	1,126	28.5	15.7
E60	64,600	4,870	36,800	10,800	26,000	24,500	9,740	7,310	484	13,600	1,159	31.8	16.9
E90	64,500	4,060	33,700	23,200	10,500	23,400	9,170	7,220	485	20,000	1,195	37.2	20.2
E120	66,100	3,270	30,600	6,600	24,000	25,500	9,760	6,900	543	14,300	1,205	33.2	17.6
E150	66,200	3,700	29,500	6,500	23,000	24,300	8,460	6,720	497	13,780	1,210	37.8	20.9
E180	76,400	4,480	28,100	8,100	20,000	27,400	8,300	6,150	651	14,100	1,236	39.6	21.8
E210	74,400	4,050	27,100	8,100	19,000	28,200	8,300	6,400	531	15,600	1,224	39.2	21.2
E240	70,800	4,420	26,200	21,000	5,200	30,000	9,290	5,910	657	16,000	1,175	30.7	16.1
E270	70,100	4,070	26,500	20,000	6,500	30,800	9,880	5,000	601	16,200	1,147	28.8	15.2
E300	75,300	4,210	25,000	23,000	2,000	32,000	9,400	5,350	612	16,800	1,160	31.3	17
E330	74,100	4,750	24,500	21,000	3,500	32,500	9,400	5,440	757	15,900	1,540	28.9	16.1
E360	77,900	4,180	24,700	22,000	2,700	35,100	7,240	6,550	752	13,300	1,440	31.4	17.7
E390	72,400	4,300	23,700	20,600	3,100	33,500	7,560	7,850	733	12,700	1,460	28.7	16.5
E420	76,300	5,320	24,300	18,900	5,400	29,800	8,670	8,550	817	13,700	1,780	32.1	18
Min	59,000	3,270	23,700	6,500	2,000	22,100	7,240	5,350	485	10,100	1,126	28.5	15.7
Mean	69,806.7	4,286	28,433.4	15,707.1	13,064.3	28,080	8,927.4	6,685.4	606.9	14,412	1,278.8	32.5	17.8
Max	77,900	5,340	42,100	23,200	32,000	35,100	11,500	9,580	817	20,000	1,780	37.2	21.8

Table 6 Concentrations of trace elements in the Sarcheshmeh copper mine tailings (all concentration are in (μg/g) except for Cu which is given in %)

Samples no. (cm)	Ag	As	Ba	Cd	Co	Cr	Cu	Hg	Mn	Li	Mo	Ni	Pb	Rb	Sr	Th	U	V	Zn	Zr
A30	0.53	34.6	457.6	0.68	34.0	44	0.15	<0.05	1,090	12.3	173	33	36.4	146.2	141	4.95	1.82	193	242.3	11
A60	0.46	32.5	465.4	0.44	33.2	48	0.13	<0.05	968	13.2	164.6	33	39.7	151.5	161.9	5.59	2.5	170	210.2	20
A90	0.34	23.8	583.9	0.14	18.8	43	0.12	<0.05	655	9.9	142	36	41.1	125.1	199.4	6.35	2.63	133	190	14
A120	0.47	20.7	613.7	1.16	24.8	29	0.11	<0.05	570	7.3	159	24	46.4	119.2	182.4	6.81	3.34	117	200.3	11
A150	0.51	23.1	561.0	1.31	24.3	28	0.10	<0.05	494	7.5	181	22	40.8	101.6	180.1	5.76	2.48	115	186	10
A180	0.33	15.3	595.1	1.60	24.9	26	0.11	<0.05	541	9.7	77.9	22	41.9	118.7	204.5	7.22	2.42	118	150.8	9
A210	0.30	16.8	622.5	0.93	19.4	31	0.13	<0.05	560	7.2	94	23	47.8	111.1	199.6	6.91	2.2	108	129.1	9
A240	0.33	21.9	647.4	1.08	23.8	34	0.12	<0.05	523	6.6	100.9	27	43.9	120.8	217.8	7.47	2.46	115	152.2	6
A270	0.36	15.7	541.4	1.35	37.4	36	0.12	<0.05	492	8.1	74.5	29	40.9	115.4	240.7	6.32	2.25	123	168.5	9
A300	0.33	15.8	653.6	1.02	28.3	31	0.13	<0.05	603	8.0	66.1	30	43.3	109.4	258.1	6.85	2.61	122	146.7	8
A330	0.28	14.2	754.1	0.65	22.5	34	0.11	<0.05	552	7.1	82.5	22	36.9	128.7	252.1	8.27	2.22	126	154.2	6
A360	0.36	15.5	532.7	0.88	31.7	43	0.13	<0.05	537	9.6	74.8	33	34.3	140.8	234.6	6.75	2.68	130	144.9	5
A390	0.27	13.4	540.8	0.96	32.2	46	0.12	<0.05	602	8.6	82.6	35	36.3	137.3	221.5	7.94	2.78	126	135.2	4
A420	0.29	16.4	563.7	1.47	34.9	53	0.11	<0.05	421	7.7	92.4	41	51.3	116.3	213.9	7.05	2.93	118	133.5	5
Min	0.27	13.4	457.6	0.14	18.8	26	0.10	<0.05	421	7.1	66.1	22	34.3	101.6	141	4.59	1.82	108	133.5	4
Mean	0.36	19.5	572.7	0.92	27.3	36.8	0.12	<0.05	601.4	8.7	108.8	28.8	41.02	122.91	203.24	6.59	2.48	128.1	165.16	8.74
Max	0.53	34.6	754.1	1.60	37.4	48	0.15	<0.05	1,090	13.2	181	41	51.3	151.5	258.1	8.27	3.34	193	242.3	20
B30	0.55	29.2	496.8	0.85	28.4	42	0.20	<0.05	885	12.5	144.6	32	48.8	135.7	145.5	5.76	2.56	196	221.1	12
B60	0.73	33.5	429.2	0.61	35.4	47	0.17	<0.05	632	11.6	137.7	38	45.5	116.8	132.3	5.36	2.4	165	230.7	17
B90	0.59	37.3	452.6	0.42	33.2	51	0.13	<0.05	685	11.6	96.7	35	38	124.6	117.6	5.87	2.6	162	205.5	12
B120	0.49	37	540.1	1.17	26.6	48	0.12	<0.05	621	10.9	94.9	33	38.8	128.4	175.1	6.86	3.05	147	186.7	10
B150	0.43	35	634.6	1.18	21.6	33	0.11	<0.05	558	8.4	129.2	24	35.1	112.7	194.1	7.36	3.34	112	164.9	11
B180	0.55	32.2	573.9	1.63	27.3	27	0.13	<0.05	532	6.5	143.8	24	45.1	117.0	176.3	6.39	2.56	111	184.1	9
B210	0.46	25.3	581.7	1.78	29.8	27	0.13	<0.05	572	8.9	109.8	24	41.8	101.8	185.3	6.50	2.35	111	178.5	9
B240	0.35	17.1	551.2	1.21	23.6	23	0.12	<0.05	602	8.3	82.8	21	40.9	102.0	180.6	6.20	2.41	105	146	8
B270	0.33	16.7	613.2	1.00	18.2	31	0.12	<0.05	458	7.5	93	23	46.7	110.4	190.1	6.78	2.35	105	122.6	7
B300	0.32	21.8	656.6	1.30	23.5	27	0.11	<0.05	400	6.8	84.3	25	53.5	107.0	216.2	7.15	2.58	109	147.6	6
B330	0.35	19	508.4	1.22	35.5	35	0.12	<0.05	461	7.3	83.9	27	48.8	108.0	210.3	5.73	2.1	121	174.9	6
B360	0.35	19.8	618.7	0.87	26.4	27	0.13	<0.05	473	6.4	84.6	23	42.7	113.2	230	7.46	2.43	109	143.4	6
B390	0.24	15.1	792.6	0.64	17.6	31	0.14	<0.05	485	6.6	75.6	26	44.7	140.3	240.7	8.39	2.29	96	115.4	5
B420	0.33	15.3	568.1	0.70	30.2	35	0.13	<0.05	598	7.6	89.7	28	39.9	156.3	215.2	7.50	2.37	128	146.1	6
Min	0.24	15.1	429.2	0.42	17.6	27	0.11	<0.05	400	6.4	75.6	21	38	101.8	117.6	5.36	2.1	96	115.4	5
Mean	0.42	24.627	563.13	1	26.33	34.06	0.13	<0.05	557.47	8.49	101.75	26.94	43.22	118.4	181.8	6.58	2.50	124.9	165.5	8.6
Max	0.73	37.3	792.6	1.78	35.5	51	0.20	<0.05	885	12.5	144.6	38	53.5	156.3	240.7	8.39	3.34	196	230.7	17
C30	0.37	17.8	497	0.60	34.0	33	0.174	<0.05	307	9.8	198.6	26	33.5	93.8	211	4.97	1.94	134	112	7
C60	0.48	18.6	514	0.79	29.8	24	0.161	<0.05	368	7.5	179	25	30.4	71.0	181	3.99	1.88	105	127	8

Table 6 continued

Samples no. (cm)	Ag	As	Ba	Cd	Co	Cr	Cu	Hg	Mn	Li	Mo	Ni	Pb	Rb	Sr	Th	U	V	Zn	Zr
C90	0.46	19.4	522	0.73	28.9	37	0.169	<0.05	286	8.6	156	27	34.7	80.1	165	4.78	2.21	113	132	6
C120	0.51	27.7	497	0.61	29.4	30	0.153	<0.05	341	8.0	164	25	42.7	80.1	160	4.42	3.03	111	147	8
C150	0.42	24	491	0.51	43.7	38	0.154	<0.05	457	8.6	146	32	46.7	73.1	157	3.57	1.95	104	172	11
C180	0.37	20.5	441	0.50	38.5	27	0.145	<0.05	534	9.2	79	26	45.8	78.9	141	4.03	1.97	113	150	9
C210	0.39	15.5	518	0.49	24.2	28	0.138	<0.05	598	9.1	147	25	34.9	83.2	157	4.61	2.21	101	132	8
C240	0.34	22.1	642	0.80	23.7	35	0.125	<0.05	578	8.4	132	29	36.9	85.8	183	5.87	2.66	111	142	7
C270	0.42	16.9	521	0.77	45.2	31	0.13	<0.05	553	8.9	99.1	27	36.8	96.5	207	4.95	2	125	156	8
C300	0.38	21.9	599	0.81	34.1	30	0.134	<0.05	519	8.3	93.1	25	38.9	102	236	6.28	2.31	116	163	8
C330	0.32	13.3	727	0.46	22.5	24	0.124	<0.05	610	8.1	75.5	20	42.9	99.3	229	6.78	2.25	117	176	9
C360	0.35	13.6	591	0.43	33.3	31	0.12	<0.05	836	9.4	88.6	26	31.7	95.1	201	5.86	2.29	117	220	7
C390	0.37	15.5	521	0.59	34.8	33	0.139	<0.05	847	9.2	102	30	32.8	100	180	5.37	2.16	116	227	7
C420	0.38	16.6	511	0.62	34.8	41	0.141	<0.05	920	9.7	93.4	33	31.5	99.8	182	5.39	2.18	122	225	11
Min	0.32	13.3	491	0.43	22.5	24	0.12	<0.05	286	7.5	75.5	20	30.4	71	141	3.57	1.88	101	112	6
Mean	0.39	18.45	538.87	0.60	31.96	31	0.14	<0.05	536	8.7	121.9	26.4	36.7	87.3	182	4.96	2.19	113.7	159.5	8
Max	0.51	27.7	727	0.81	43.7	41	0.174	<0.05	920	9.8	198.6	33	46.7	102	236	5.87	3.03	134	227	11
D30	0.42	27	339	1.43	48.7	39	0.242	<0.05	770	12.4	137	43	34.6	103	122	4.41	1.83	156	204	5
D60	0.47	25.4	364	0.94	31.9	39	0.238	<0.05	446	9.8	125	33	37.4	90.5	146	4.90	2.7	131	206	6
D90	0.44	26.7	449	0.37	27.4	23	0.209	<0.05	294	8.1	103	21	34	101	187	5.48	2.4	112	207	6
D120	0.39	22.9	547	0.93	22.6	22	0.204	<0.05	285	7.2	96.3	21	39.3	98.0	174	6.46	2.25	89	215	8
D150	0.61	25.9	480	1.06	25.6	20	0.2	<0.05	334	7.1	186	24	44.3	92.1	151	5.81	2.24	86	204	7
D180	0.46	29.9	399	1.02	29.2	27	0.165	<0.05	461	7.8	139	27	47.3	90.0	134	4.72	2	91	187	9
D210	0.38	20.5	343	0.39	43.3	20	0.135	<0.05	436	8.0	59.6	26	47.7	85.7	110	4.03	1.61	91	160	12
D240	0.43	19.3	346	1.01	42.7	21	0.132	<0.05	522	8.6	65.1	28	49.8	85.4	101	4.17	1.73	102	177	14
D270	0.38	18.3	479	0.72	20.6	35	0.116	<0.05	476	7.2	119	20	54.4	104	142	5.84	2.21	87	146	11
D300	0.38	23.8	527	0.84	20.4	16	0.114	<0.05	424	5.4	109	21	49.5	99.9	170	7.42	2.81	76	165	10
D330	0.35	23.3	520	0.97	20.9	18	0.114	<0.05	348	5.8	99.7	21	42.1	98.6	208	7.60	2.64	81	159	8
D360	0.30	20.1	545	0.80	21.6	17	0.104	<0.05	347	5.8	94.6	20	43.4	113	215	8.47	2.56	83	153	9
D390	0.32	13.2	585	0.50	23.8	18	0.1197	<0.05	407	6.8	56.5	22	40.1	115	197	7.73	2.89	83	157	9
D420	0.32	11.8	522	0.36	24.3	17	0.1095	<0.05	561	6.2	92	21	31.6	110	164	8.66	2.42	79	194	8
Min	0.30	11.8	339	0.37	20.4	16	0.104	<0.05	285	5.4	56.5	20	31.6	85.4	101	4.03	1.61	76	146	5
Mean	0.39	21.32	452.3	0.78	28.2	23.2	0.153	<0.05	426.4	7.4	102.5	24.5	41.8	98.1	154.8	5.98	2.26	94.86	178.7	8.47
Max	0.61	29.9	585	1.43	48.7	39	0.242	<0.05	770	12.4	186	43	54.4	115	215	8.66	2.89	156	215	14
E30	0.67	33.2	311	0.50	29.0	30	0.234	<0.05	692	9.4	134	33	47.8	104	110	3.81	1.67	129	226	6
E60	0.43	24	376	0.96	30.3	31	0.1908	<0.05	572	8.8	65.7	29	38.5	99.6	138	5.48	2.32	114	176	6
E90	0.36	19.4	392	0.84	30.1	27	0.16	<0.05	537	8.8	51.1	27	40.3	110	169	6.18	2.33	103	154	8
E120	0.40	17.6	369	1.00	40.5	26	0.121	<0.05	507	8.7	62.2	25	37.7	125	177	5.55	2.34	121	187	9

Table 6 continued

Samples no. (cm)	Ag	As	Ba	Cd	Co	Cr	Cu	Hg	Mn	Li	Mo	Ni	Pb	Rb	Sr	Th	U	V	Zn	Zr
E150	0.41	14.8	488	0.94	22.0	23	0.122	<0.05	409	6.5	90.9	23	36.2	113	181	7.05	3.1	92	183	7
E180	0.39	14.7	542	0.87	24.9	33	0.128	<0.05	492	9.2	78.4	24	34.8	107	204	6.10	2.46	127	150	6
E210	0.51	22.9	614	1.08	26.2	28	0.132	<0.05	489	8.1	131	24	43.3	112	193	7.27	2.25	106	141	8
E240	0.46	28	474	0.97	30.8	37	0.132	<0.05	624	9.6	119	27	43.2	92.7	152	4.94	2.09	126	151	9
E270	0.37	17.5	433	0.87	37.3	24	0.127	<0.05	598	9.1	61.9	24	36.5	110	127	4.84	1.85	116	161	10
E300	0.38	18.6	471	0.90	37.6	23	0.111	<0.05	634	9.7	68.3	23	37.2	131	139	5.13	1.98	120	166	8
E330	0.35	21.1	552	0.91	35.9	27	0.137	<0.05	650	8.4	82.9	24	53.7	89.6	160	5.16	1.93	129	156	10
E360	0.27	22.3	698	0.97	19.2	25	0.123	<0.05	305	7.2	79.3	21	50.1	84.9	210	6.33	2.26	114	114	5
E390	0.31	22.4	670	0.70	20.8	19	0.135	<0.05	313	6.9	104	18	45.2	84.5	210	5.84	2.12	98	158	6
E420	0.32	23.8	610	1.00	26.1	24	0.142	<0.05	483	7.5	133	22	30.7	83.6	244	5.80	2.21	118	205	8
Min	0.27	14.7	311	0.50	19.2	19	0.111	<0.05	305	6.5	51.1	18	30.7	83.6	110	3.81	1.67	92	114	5
Mean	0.39	21	487.4	0.87	28.66	26.4	0.14	<0.05	507.4	8.3	87.52	24.14	40.39	102.03	168.27	5.55	2.17	113.7	162.8	7.4
Max	0.67	33.2	698	1.08	37.6	37	0.234	<0.05	692	9.7	134	33	50.1	131	244	6.33	3.1	129	226	10

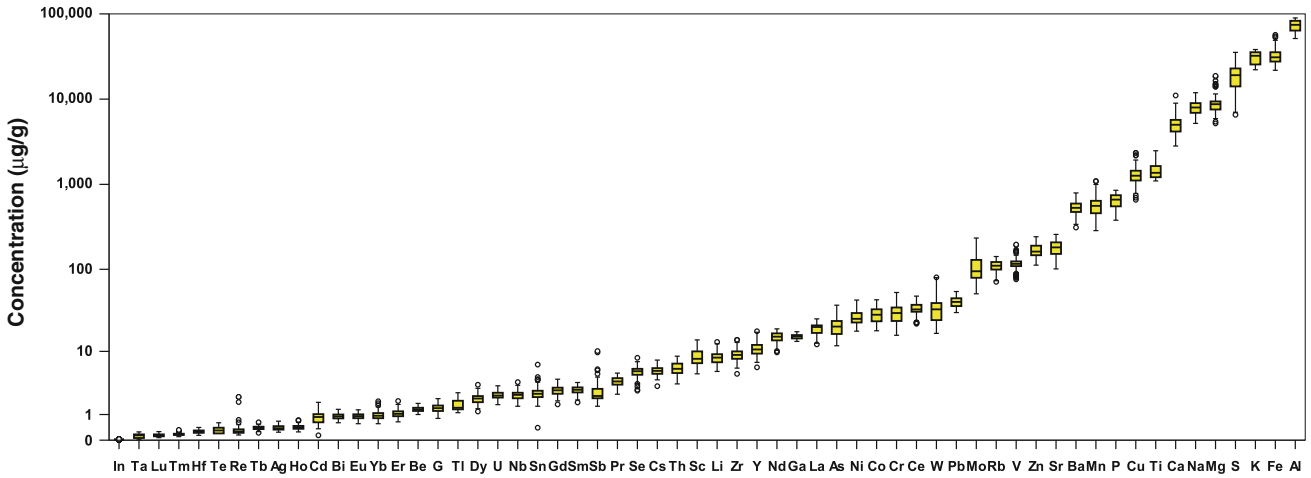

Fig. 8 Bulk concentrations of 60 elements in 70 solid samples of the Sarcheshmeh copper mine tailings

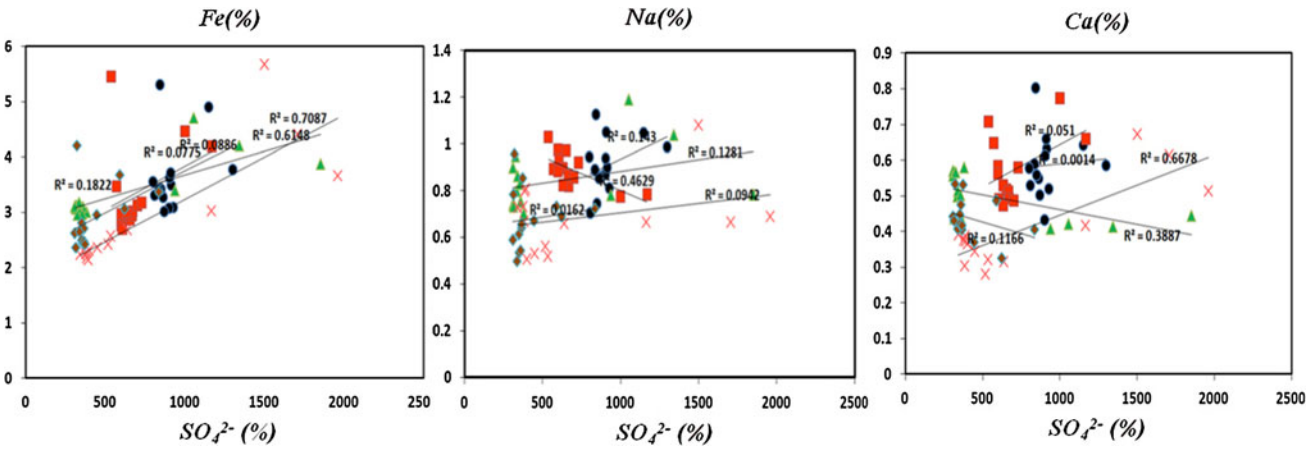

Fig. 9 Fe, Na and Ca concentrations (wt %) plotted versus SO_4^{-2}concentration (mg/L) in tailings. *Filled circles* indicate A, *filled square* show B, *filled triangles* indicate C, *filled diamonds* indicate D and *crossed line* indicate E profiles

weak positive correlation ($r = 0.225$) in the profile B, a strong positive correlation ($r = 0.81$) in the profile D and a negative moderate correlation in the profiles C and E ($r = -0.623$ and -0.341), respectively. The SO_4^{2-} concentration reveals a positive moderate correlation with Na ($r = 0.378$, 0.358 and 0.307) in the profiles A, C and D respectively, a weak correlation ($r = 0.127$) in the profile E and an almost moderate negative correlation in the profile B ($r = -0.680$). The SO_4^{2-} concentration illustrates a positive weak correlation with Fe ($r = 0.297$, 0.278) in the profiles A, B respectively, a moderate correlation ($r = 0.427$) in the profile E and a strong positive correlation ($r = 0.784$ and 0.841) in the profiles C and D, respectively. The positive correlation between SO_4^{2-} and Fe in the tailings surface layers indicates that major amount of Fe are most likely associated with sulphide phases. In general, the concentrations of Ca and Na increased with increasing the SO_4^{2-} concentration of solid phase in the tailings samples probably representing that these elements might be associated with the presence of sulphate minerals. Gypsum, hydrous iron oxide (goethite) and Fe-hydroxides are probably the most common secondary minerals resulted from pyrite oxidation in the oxidised zone of the tailings. In the tailings solid samples, $CuSO_4$, $Fe_2(SO_4)_3$, $MgSO_4$ and Al_2O_3 are new major formed minerals.

Figure 10 shows the relationships between the bulk concentrations of some elements and paste pH values. Table 7 presents the correlation between some major and trace elements and paste pH in the five profiles investigated in this study.

A negative correlation was observed between Fe and paste pH due to an increase in Fe concentration under low pH value up to pH = 5. However, the correlation between Fe and pH is somewhat positive for high pH values (above 5). The change in the correlation between pH and Fe is due to the fact that various compounds may control Fe

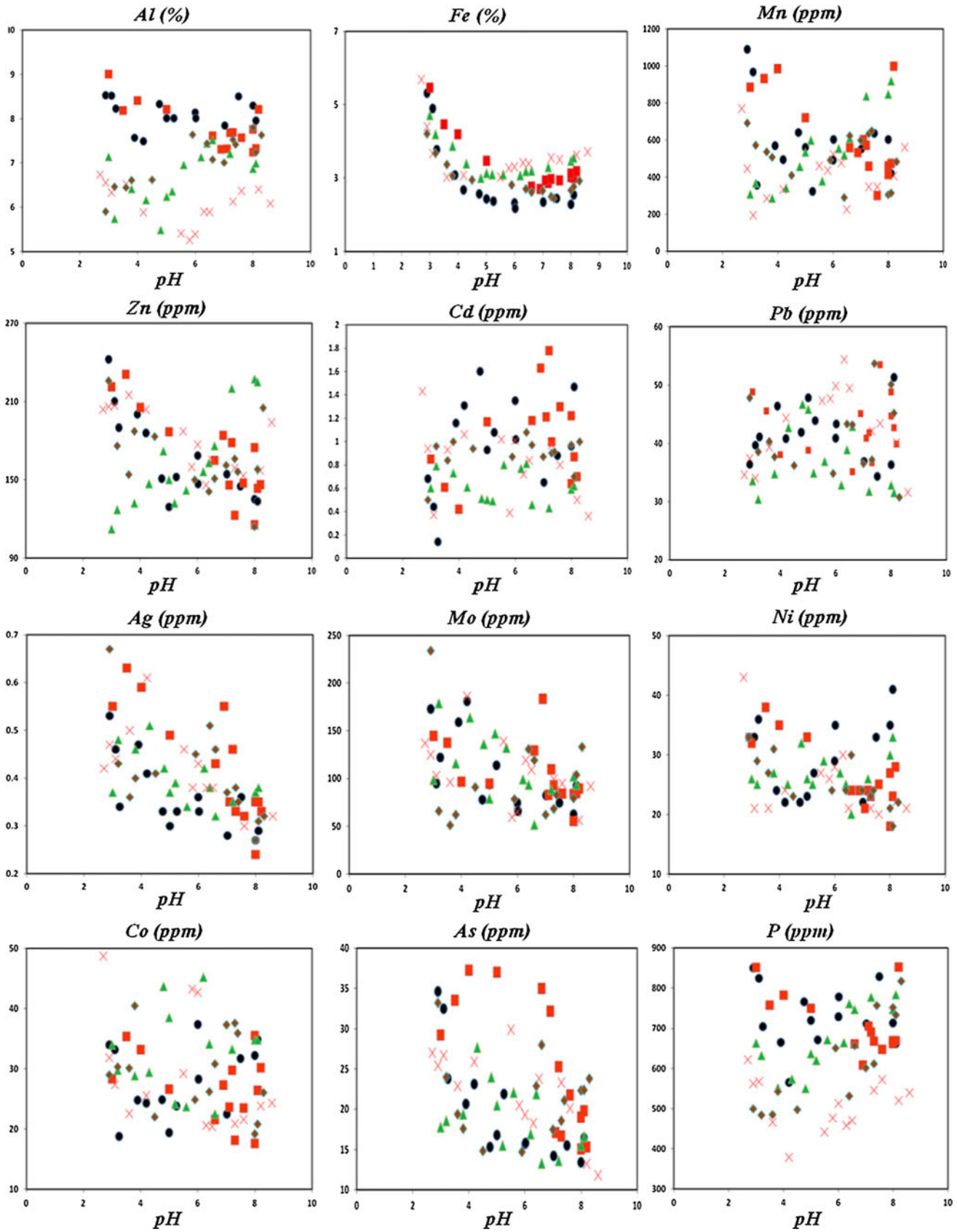

Fig. 10 Bulk concentrations of some elements in tailings samples as a function of the paste pH values. *Filled circles* indicate A, *filled square* show B, *filled triangles* indicate C, *filled diamonds* indicate D and *crossed line* indicate E profiles

Table 7 The correlation between pH and major and trace elements given for various profiles

Element	pH in various profiles				
	A	B	C	D	E
Al	–	SC	MC	WC	SC
		−0.77	0.55	−0.3	−0.88
Fe	MC	SC	SC	SC	SC
	−0.37	−0.8	−0.79	−0.87	−0.91
Mn	MC	MC	SC	–	MC
	−0.38	−0.67	0.9		−0.32
Zn	SC	SC	SC	SC	MC
	−0.8	−0.85	0.9	−0.73	−0.46
Cd	MC	MC	WC	MC	WC
	0.37	0.35	−0.21	−0.44	26
Pb	–	–	–	WC	WC
				0.24	−0.15
Ag	SC	SC	MC	SC	MC
	−0.74	−0.85	−0.55	−0.73	−0.6
Mo	MC	MC	MC	MC	WC
	−0.67	−0.48	−0.54	−0.5	−0.11
Ni	WC	SC	WC	MC	SC
	0.26	−0.82	0.28	−0.54	−0.77
Co	WC	MC	WC	MC	WC
	0.3	−0.4	0.1	−0.43	–0.2
As	SC	SC	MC	SC	WC
	−0.8	−0.75	−0.45	−0.75	−0.14
Ga	–	SC	–	–	MC
		−0.77			−0.6
P	WC	MC	SC	NC	SC
	−0.11	−0.56	0.78	−0.06	0.87

WC Weak correlation, *MC* moderate correlation, *SC* strong correlation, *NC* no correlation

solubility over a wide range of pH. Concentrations of some metal cations (Zn, Cd and Pb) were low under acidic conditions (in oxidised zone of tailings) because of the enhancement of metal dissolution, while metal release decreased with the increasing pH under near neutral conditions (in unoxidised zone).

Investigations carried out by Finkelman (1994) revealed that the pyrite oxidation may release trace elements to the environment. This matter was considered in this research. Figures 11, 12 and 13 show the distributions of major (Fe, S, Al, Ca, Mg, Na and K), trace (Mo, Sr, Zr, Ni, Mn, Pb, Zn, Ag, As, Cu, Rb and Cd) and few rare earth elements (La, Ce and Nd) in the profiles A, B, C, D and E against depth. Several geochemical trends were observed in the depth profiles. Sulphur (S) increased with increasing depth due to the leaching process resulted by pyrite oxidation in the tailings. The maximum concentrations of S were observed at about 0.5 m depth of almost all profiles. Al increased with increasing depth of the tailings profile. Fe had initially a decreasing trend up to 2.5 m. Below this depth, it increased slightly. K remained constant throughout the tailings profile. Na, Ca and Mg show initially a decreasing trend in the oxidised zone up to 0.9, 1.2 and 1.4 m respectively; followed by almost a constant trend with increasing depth of all profiles (unoxidsed zone). The decrease in concentration of these elements with depth may be due to the mobility restrictions of a Ca- and Na-bearing complex, evaporation of pore waters containing elevated concentrations of Ca, Na and Mg near the tailings surface and formation of gypsum.

Three different trends can be seen in the distributions of elements at the tailings profiles:

1. Elements including Zn, Pb, Rb, U, Hf, Nd, Zr and Ga show almost a constant trend with depth.
2. Elements comprising Cd, Sr, Th, La and Ce increased with increasing depth of the tailings materials.
3. Elements including Co, V, Ti, Cr, Cu, As, Mn, Ag, Mo and Ni exhibit initially a decreasing trend from tailings surface to the depths that vary between 0.9 and 1.2. They then remained constant with depth.

The maximum concentrations of As were observed at 0.3, 0.9, 1.2, 1.5 and 2.1 m depths of the profiles A, B, C, D and E, respectively. The maximum concentrations of Al were observed at depths of 4.2, 4, 3.3, 4.2, and 2.4 m in the profiles A, B, C, D and E, respectively. The results further indicate that the peak concentrations of Al, Cd, Ni, Pb, Rb, Hf, Zr, La, Ce, Cu, Mn, Mo, Ti, Zn, As, Ag, Cr, Co and V were observed at depth intervals 3.6–4.2, 3.6–4.2, 3.9–4.2, 2.7–3.3, 3.6–4.2, 2.4–3, 3.9–4.2, 3.9–4.2, 3.6–4.2, 0.3–0.6, 0–0.6, 0.3–0.6, 0.3–0.6, 0.3–0.9, 0.3–1.8, 0.3–1.5, 3.9–4.2, 2.1–3 and 0.3–0.6 m, respectively.

Conclusions

This paper describes a joint geochemical–mineralogical study on sulphide minerals, in particular pyrite and chalcopyrite oxidation in a large tailings impoundment of the Sarcheshmeh porphyry copper mine. These minerals in the tailings have oxidised, with pyrite oxidation progressing deeper in the tailings profile than chalcopyrite oxidation. Pyrite oxidation decreased steadily and chalcopyrite oxidation reduced sharply at lower depths, up to 1.5 m depth, where the oxygen diffusion decreases rapidly. Below this depth, oxidation process gradually decreased, and it entirely ceased at an approximate depth of 3.5 m. The tailings contain about 4–6 wt % pyrite and 0.1–0.3 chalcopyrite. Calcite, quartz, muscovite-illite, chlorite, albite, orthoclase, halite and dolomite are the dominant gangue

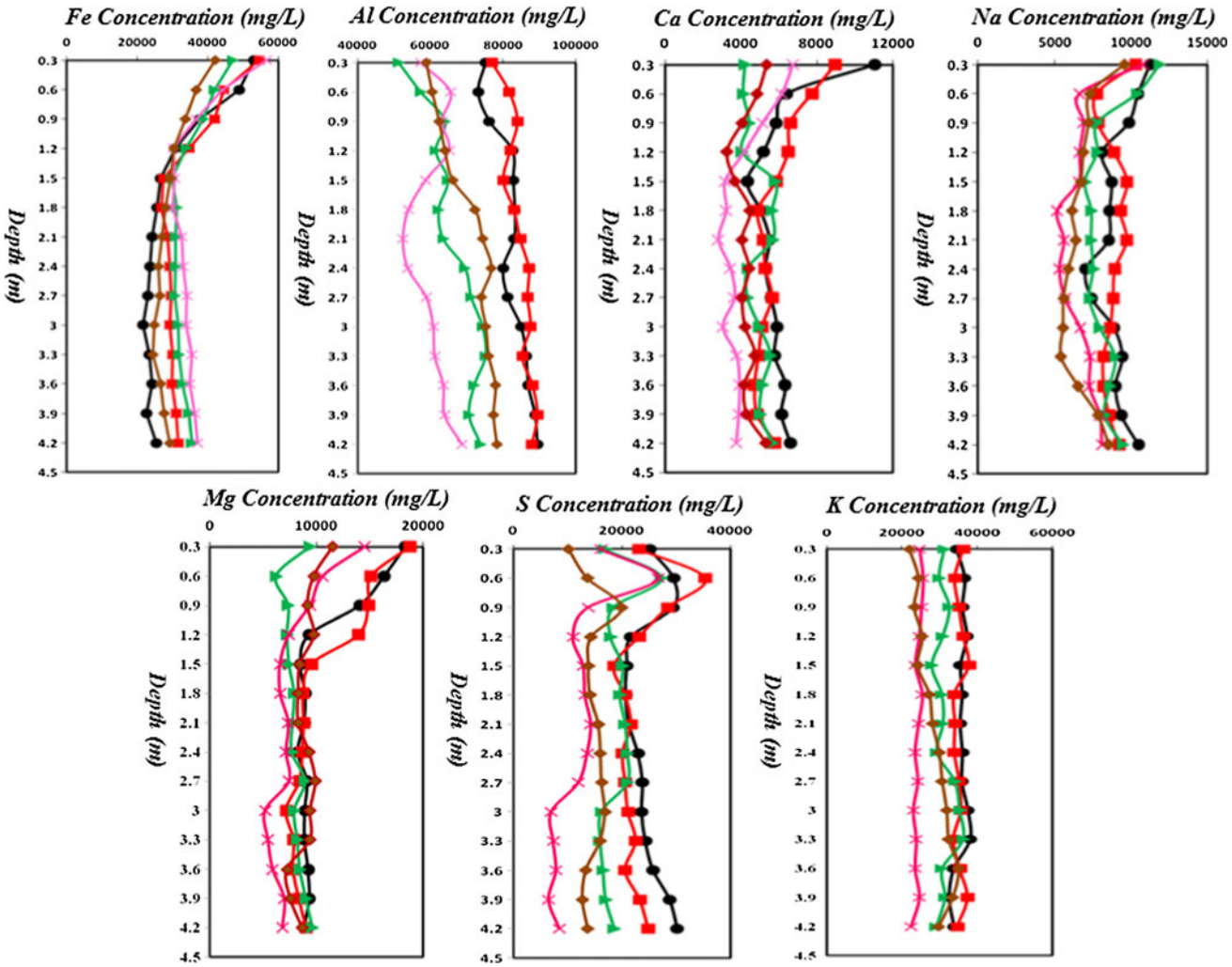

Fig. 11 Depth profiles of Fe, Al, Ca, Na, Mg, S and K (wt %) for the profiles A, B, C, D and E in the tailings materials. *Filled circles* indicate A, *filled square* show B, *filled triangles* indicate C, *filled diamonds* indicate D and *crossed line* indicate E profiles

minerals in the tailings impoundments. The oxidation process caused elevated concentrations of SO_4^{2-}, iron and trace elements. A maximum concentration of 1,960 mg/L was observed for SO_4^{2-} at a depth of 0.9 m in tailings profile. $Fe_2(SO_4)_3$, $CuSO_4$, $MgSO_4$ and $MnSO_4$ were the main secondary sulphate minerals in the tailings. The sulphide minerals' oxidation in tailings has lowered the pH of the materials below 3. The concentration of HCO_3^- in the solid samples was very low. A zero concentration was measured for CO_3^{2-}. Cu (0.1–0.242 %), Mn (285–1,090 ppm), Ba (311–792.6 ppm), Sr (110–258.1 ppm), Zn (112–243.2 ppm), Mo (51.1–198.6 ppm), V (76–196 ppm), Rb (71–156.3 ppm), Pb (30.4–54.4 ppm), Ni (18–43 ppm), As (11.8–37.3 ppm), Li (5.4–13.2 ppm) and Ag (0.24–0.73 ppm) are the most abundant trace elements in the tailings; although the distribution of these elements differs at various depths of the tailings. The tailings impoundment has a high acid-producing potential and low acid-neutralising potential. Determining the acid-producing minerals (both primary and secondary) and the acid-neutralising minerals in tailings materials is a crucial task to predict geochemical mobility of potentially toxic elements through the tailings. Furthermore, performing a combination of detailed mineralogical and geochemical studies facilitates development of an accurate tailings management programme as a way to better understand and predict the complex geochemical interactions involved in AMD generation. The results obtained from this investigation can provide useful information for designing an appropriate remediation strategy to prevent metal release to soil and water resources. Developing a site reclamation and environmental management programme in the Sarcheshmeh tailings impoundment will limit environmental problem.

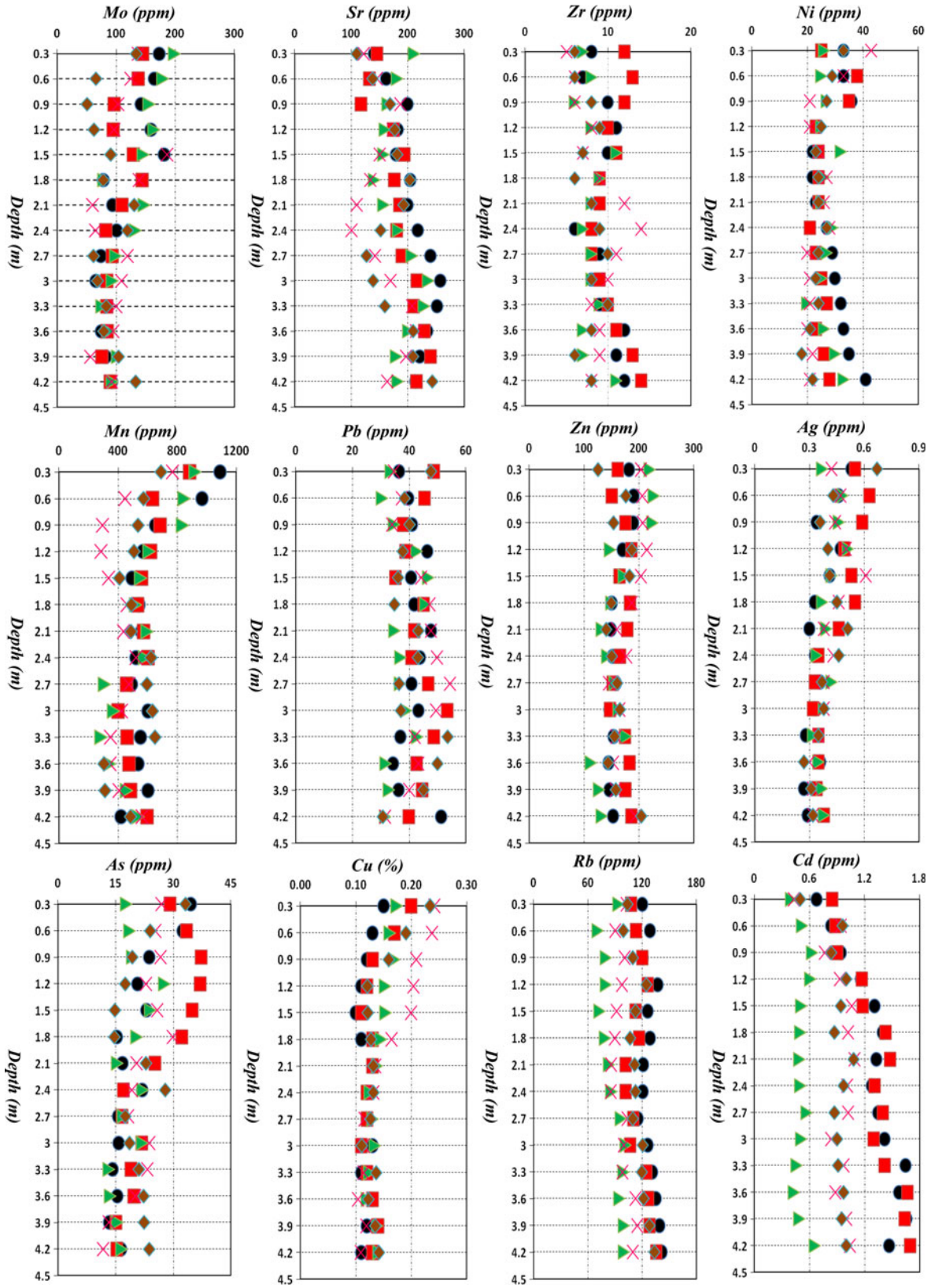

Fig. 12 Depth profiles of Mo, Sr, Zr, Ni, Mn, Pb, Zn, Ag, As, Cu, Rb and Cd for the profiles A, B, C, D and E in the tailings. *Filled circles* indicate A, *filled square* show B, *filled triangles* indicate C, *filled diamonds* indicate D and *crossed line* indicate E profiles

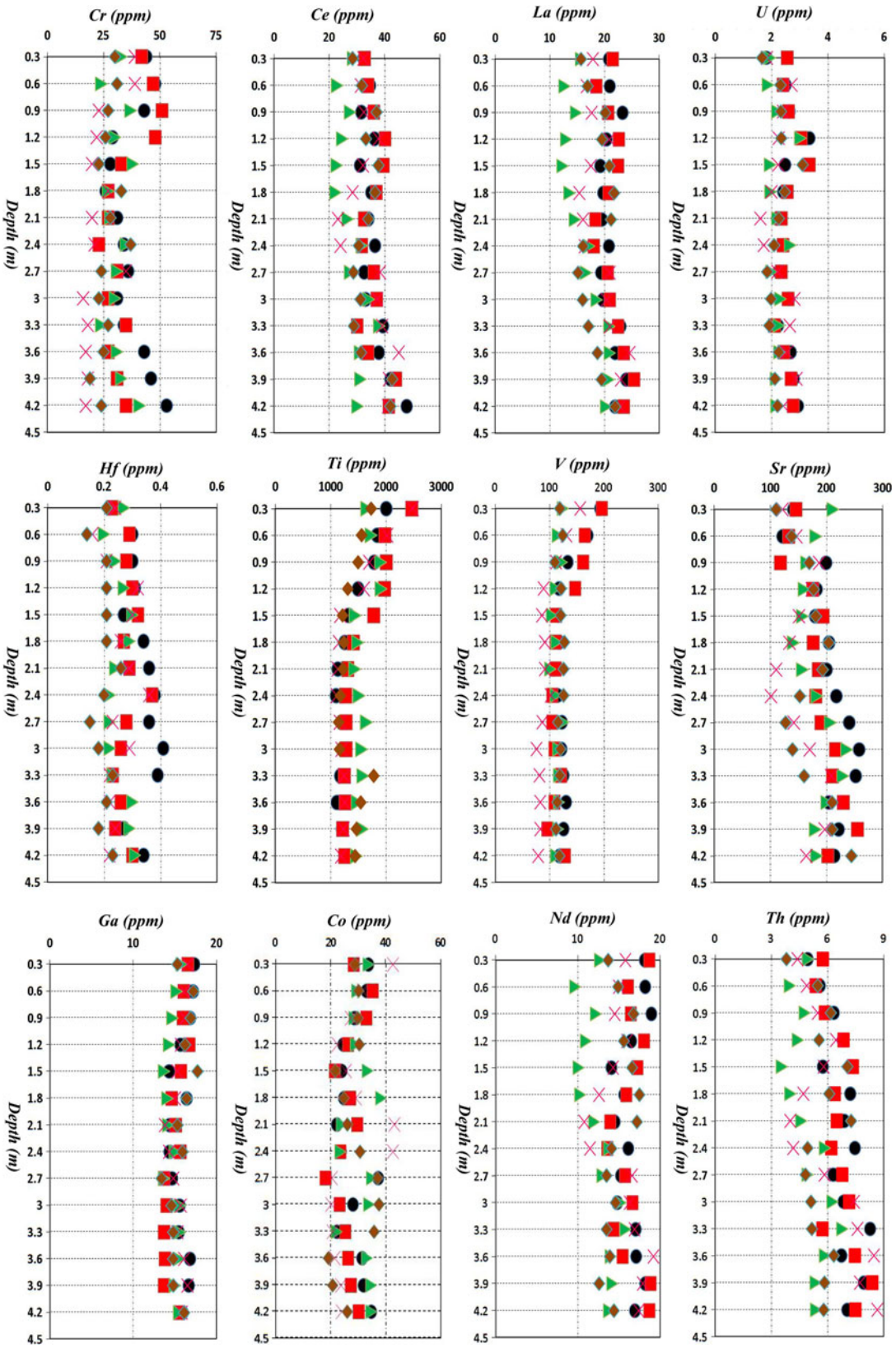

Fig. 13 Depth profiles of Cr, Ce, La, U, Hf, Ti, V, Sr, Ga, Co, Nd and Th for the profiles A, B, C, D and E in the tailings. *Filled circles* indicate A, *filled square* show B, *filled triangles* indicate C, *filled diamonds* indicate D and *crossed line* indicate E profiles

Acknowledgments The author would you like to thanks the National Iranian Copper Industries Company (NICICo.) to funding this research project. Many thanks are due to Shahrood University of Technology for laboratory analyses.

References

Adam K, Kourtis A, Gazea B, Kontopoulos A (1997) Evaluation of static tests used to predict the potential for acid drainage generation at sulphide mine sites. Trans Inst Min Metall Sect A Min Ind 106:1–50

Ariafar A, Gholami R, Rooki R, Doulati Ardejani F (2012) Heavy metal pollution assessment using support vector machine in the Shur River, Sarcheshmeh copper mine, Iran. Environ Earth Sci 67:1191–1199

Atkins AS, Pooley FD (1982) The effects of bio-mechanisms on acidic mine drainage in coal mining. Int J Mine Water 1:31–44

Banisi S, Finch JA (2001) Testing a floatation column at the Sarcheshmeh copper mine. Mineral Eng 14(7):785–789

Banks SB, Banks D (2001) Abandoned mines drainages: impact assessment and mitigation of discharges from coal mines in the UK. Eng Geol 60:31–37

Blowes DW, Ptacek CJ, Jambor JL, Weisener CG (2003) The Geochemistry of Acid Mine Drainage. In: Treatise on Geochemistry, vol 9. Elsevier, Oxford, pp 149–204

Canovas CR, Olias M, Nieto JM, Sarmiento AM, Ceron JC (2007) Hydrogeochemical characteristics of the Tinto and Odiel Rivers (SW Spain). Factors controlling metal contents. Sci Total Environ 373:363–382

Dinelli E, Lucchhini F, Fabbri M, Cortecci G (2001) Metal distribution and environmental problems related to sulfide oxidation in the Libiola copper mine area (Ligurian Apennines, Italy). J Geochem Explor 74:141–152

Doulati Ardejani F, Karami GH, Assadi AB, Dehghan RA (2008a) Hydrogeochemical investigations of the Shour River and groundwater affected by acid mine drainage in Sarcheshmeh porphyry copper mine. 10th international mine water association congress, Karlovy Vary, Czech Republic, pp 235–238

Doulati Ardejani F, Jodeiri Shokri B, Moradzadeh A, Soleimani E, Ansari Jafari M (2008b) A combined mathematical geophysical model for prediction of pyrite oxidation and pollutant leaching associated with a coal washing waste dump. Int J Environ Sci Tech 5(4):517–526

Dutrizac JE, MacDonald RJC (1973) The effect of some impurities on the rate of chalcopyrite dissolution. Can Metall Quart 12(4): 409–420

Eggleston Carrick M, Ehrhardt JJ, Stumm W (1996) Surface structural controls on pyrite oxidation kinetics: an XPS-UPS, STM, and modeling study. Am Miner 81:1036–1056

Equeenuddin SK, Md Tripathy, Sahoo SPK, Panigrahi MK (2010) Hydrogeochemical characteristics of acid mine drainage and water pollution at Makum Coalfield, India. J Geochem Explor 105:75–82

Erickson PM, Kleinmann RLP, Posluszny ET, Leonard-Mayer PJ (1982) Hydrogeochemistry of a large mine pool. Proceedings of the first international mine water congress of the international mine water association (IMWA), Budapest, Hungary, 19–24 April, pp 27–42

Evangelou VP (1995) Potential microencapsulation of pyrite by artificial inducement of $FePO_4$ coatings. In: International land reclamation and mine drainage conference and the third international conference on the abatement of acid drainage, Pittsburgh 2, pp 96–103

Evangelou VP, Zhang YL (1994) A review: pyrite oxidation mechanisms and acid mine drainage prevention. Environ Sci Tech 25:141–199

Finkelman RB (1994) Modes of occurrence of potentially hazardous elements in coal: levels of confidence. Fuel Process Technol 39(1–3):21–34

Gholami R, Ziaii M, Ardejani FD, Maleki Sh (2011a) Specification and prediction of nickel mobilization using artificial intelligence methods. Cent Eur J Geosci 3(4):375–384

Gholami R, Kamkar-Rouhani A, Ardejani FD, Maleki Sh (2011b) Prediction of toxic metals concentration using artificial intelligence techniques. Appl Water Sci 1:125–134

Gladfelter WL, Dickerhoof DW (1976) Use of atomic absorption spectrometry for iron determinations in coals. Fuel 55(4): 360–361

Hiroyoshi N, Hirota M, Hirajima T, Tsunekawa M (1997) A case of ferrous sulfate addition enhancing chalcopyrite leaching. Hydrometallurgy 47:37–45

Jambor JL (1994) Mineralogy of sulfide-rich tailings and their oxidation products. In: Jambor JL, Blowes DW (eds) The Environmental Geochemistry of Sulfide Mine-wastes, Short Course Handbook 22, Mineralogical Association of Canada, May 1994. Waterloo, Ontario, pp 59–102

Jang HJ, Wadsworth ME (1994) Kinetics of hydrothermal enrichment of chalcopyrite. In: Alpers CN, Blowes DW (eds) Environmental geochemistry of sulfide oxidation, ACS Symposium Series. American Chemical Society, Washington, DC, p 661

Jannesar Malakooti S, Noaparast M, Tonkaboni SZS, Ardejani FD, Soleimani E, Esmaeilzadeh E (2012) Mineralogical and geochemical studies on pyrite and chalcopyrite oxidations in the Sarcheshmeh copper mine tailings. International Mine Water Association Conference, Annual Conference 2012, 30 September–4 October, Bunbury, Western Australia, pp 223–230

Kim JY, Chon HT (2001) Pollution of a water course impacted by acid mine drainage in the Imgok creek of the Gangreung coal field, Korea. Appl Geochem 16:1387–1396

Kovács E, Tamás J, Frančišković-Bilinski S, Omanović D, Bilinski H, Pižeta I (2012) Geochemical study of surface water and sediment at the abandoned Pb-Zn mining site at Gyongyosorosz, Hungary. J Fresenius Environ Bull 21:1212–1218

Lee JS, Chon HT (2006) Hydrogeochemical characteristics of acid mine drainage in the vicinity of an abandoned mine, Daduk Creek, Korea. J Geochem Explor 88:37–40

Marandi R, Doulati Ardejani F, Amir Afshar H (2010) Biosorption of lead (II) and zinc (II) ions by pre-treated biomass of phanerochaete chrysosporium. J Min Environ 1(1):9–16

Moncur MC, Ptacek CJ, Blowes DW, Jambor JL (2005) Release, transport and attenuation of metals from an old tailings impoundment. Appl Geochem 20:639–659

Morin KA, Cherry JA, Dave NK, Lime TP, Vivjurka AJ (1988) Migration of acidic groundwater seepage from uranium-tailing impoundments, 1. Filed study and conceptual hydrogeochemical model. J Contaminant Hydrol 2:271–303

Plumlee GS (1999) The environmental geology of mineral deposits. In: Plumlee GS, Logsdon MJ (eds) The environmental geochemistry of ore deposits. Part A: processes, techniques, and health issues. Reviews in economic geology, pp 71–116

Ricca VT, Schultz RR (1979) Acid mine drainage modelling of surface mining. In: Argall GO, Brawner CO Jr (eds) Proceedings of the first international mine drainage symposium. Miller-Freeman Publications, San Francisco, pp 651–670

Rimstidt JD, Chermak JA, Gagen PM (1994) Rates of Reaction of Galena, Spalerite, Chalcopyrite, and Asenopyrite with Fe(III) in Acidic Solutions. In: Alpers CN, Blowes DW (eds) Environmental Geochimistry of Sulfide Oxidation, ACS Symposium Series. American Chemical Society, Washington, pp 2–13

Rooki R, Doulati Ardejani F, Aryafar A, Bani Asadi A (2011) Prediction of heavy metals in acid mine drainage using artificial neural network (ANN) from the Shur River of the Sarcheshmeh porphyry copper mine, Southeast Iran. Environ Earth Sci 64:1303–1316

Rubio RF, Del Olmo AG (1995) Mining drainage and water supply under sustainable constraints. In: Hotckkiss WR, Downey JS, Gutentag ED, Moore JE (eds) Proceedings on water resources at risk, American Institute of Hydrology, Denver, 14–18 May, pp 23–32

Schippers A, Kock D, Schwartz M, Böttcher ME, Vogel H, Hagger M (2007) Geomicrobiological and geochemical investigation of pyrrhotite-containing mine waste tailing dam near Selebi-Phikwe in Botswana. J Geochem Explor 92:151–158

Seifpanahi Shabani K, Ardejani FD, Singh RN, Marandi R, Soleimanyfar H (2011) Numerical Modeling of Cu^{2+} and Mn^{2+} ions biosorption by *Aspergillus Niger* fungal biomass in a continuous reactor. Arch Min Sci 56(3):461–476

Shafaei Tonkaboni SZ, Malakooti SJ, Ardejani FD, Singh RN, Soleimani E, Noaparast M, Naseh R (2011) Pyrite oxidation in the Sarcheshmeh copper mine tailings dam, Kerman, Iran. In: Proceedings of the 11th congress of the International Mine Water Association, pp 59–64

Shahabpour J, Doorandish M (2008) Mine drainage water from the Sarcheshmeh porphyry copper mine, Kerman, IR Iran. Environ Monit Assess 141:105–120

Shahhoseiny M, Doulati Ardejani F, Shafaei SZ, Noaparast M, Hamidi D (2013) Geochemical and mineralogical characterization of a pyritic waste pile at the Anjir Tangeh coal washing plant, Zirab, Northern Iran. Mine Water Environ. doi: 10.1007/s10230-013-0219-7

Singer PC, Stumm W (1970) Acidic mine drainage: the rate determining step. Science 167:1121–1123

Soleimanifar H, Doulati Ardejani F, Marandi R (2011) Bio-remediation of acid mine drainage in the Sarcheshmeh porphyry copper mine by Fungi: batch and fixed bed process. Int J Min Geo-Eng 45(1):87–102

Stumm W, Morgan J (1996) Aquatic chemistry: chemical equilibria and rates in natural waters. Willey, New York, p 1022

Walter AL, Frind EO, Blowes DW, Ptacek CJ, Molson JW (1994a) Modelling of multicomponent reactive transport in groundwater, 1. Model development and evaluation. Water Resour Res 30(11):3137–3148

Walter AL, Frind EO, Blowes DW, Ptacek CJ, Molson JW (1994b) Modelling of multicomponent reactive transport in groundwater, 2. Metal mobility in aquifers impacted by acidic mine water discharge. Water Resour Res 30(11):3149–3158

Waterman GC, Hamilton RL (1975) The Sar Cheshmeh porphyry copper deposit. Economic Geol 70:568–576

Williams RE (1975) Waste production and disposal in mining, milling, and metallurgical industries. Miller-Freeman Publishing Company, San Francisco, p 485

Williamson MA, Rimstidt JD (1994) The kinetics and electrochemical rate-determining step of aqueous pyrite oxidation. Geochim Cosmochim Acta 58:5443–5454

Wu P, Tang Ch, Liu C, Zhu L, Pei TQ, Feng L (2009) Geochemical distribution and removal of As, Fe, Mn and Al in a surface water system affected by acid mine drainage at a coalfield in Southwestern China. Environ Geol 57:1457–1467

Zhao FH, Cong ZY, Sun HF, Ren DY (2007) The geochemistry of rare earth elements (REE) in acid mine drainage from the Sitai coal mine, Shanxi Province, North China. Int J Coal Geol 70(1–3):184–192